Journal of Geophysical Research: Space Physics

RESEARCH ARTICLE
10.1029/2018JA025312

Thermal and Energetic Ion Dynamics in Ganymede's Magnetosphere

A. R. Poppe[1], **S. Fatemi**[2], **and K. K. Khurana**[3]

[1]Space Sciences Laboratory, University of California, Berkeley, CA, USA, [2]Swedish Institute of Space Physics, Kiruna, Sweden, [3]Institute for Geophysics and Planetary Physics, University of California, Los Angeles, CA, USA

Key Points:
- Thermal and energetic ion tracing is performed using hybrid simulations of Ganymede's magnetosphere
- Surface ion fluxes are concentrated in Ganymede's poles, with additional energetic ion precipitation in equatorial region
- We discuss implications for surface weathering and exospheric generation at Ganymede by ion irradiation

Correspondence to:
A. R. Poppe,
poppe@ssl.berkeley.edu

Citation:
Poppe, A. R., Fatemi, S., & Khurana, K. K. (2018). Thermal and energetic ion dynamics in Ganymede's magnetosphere. *Journal of Geophysical Research: Space Physics*, *123*. https://doi.org/10.1029/2018JA025312

Received 3 FEB 2018
Accepted 10 MAY 2018
Accepted article online 16 MAY 2018

Abstract Ganymede is the solar system's only known moon with an intrinsic, global magnetic field. This field is strong enough to stand off the incident Jovian magnetospheric flow to form a small, complex magnetosphere around the satellite. Ganymede's magnetosphere is thought to be responsible for variable surface weathering patterns, the production of a neutral exosphere, and the generation of UV aurorae near Ganymede's open-closed field line boundaries; however, the exact details and underlying mechanisms are poorly understood. We use results from three-dimensional hybrid models of Ganymede's magnetosphere and a three-dimensional particle tracing model to quantify the dynamics of thermal and energetic Jovian ions as they interact with Ganymede's magnetosphere and precipitate to the surface. We identify the formation of quasi-trapped ionic radiation belts in the model and variable surface weathering. Most of the particle precipitation occurs in Ganymede's polar caps, yet ions also precipitate onto Ganymede's equatorial region in lesser amounts due to particle shadowing of quasi-trapped ions in Ganymede's ionic radiation belts. Model results predict that within Jupiter's central plasma sheet, total ion fluxes to Ganymede's polar, leading, and trailing hemispheres are 50×10^6, 10×10^6, and 0.06×10^6 cm$^{-2} \cdot$ s^{-1}, respectively. Finally, convolution of incident ions fluxes with neutral sputtering yields for icy bodies predicts neutral sputtered fluxes in Ganymede's polar, leading, and trailing hemispheres of 1.3×10^9, 4.8×10^8, and 1.2×10^8 neutrals cm$^{-2} \cdot$ s^{-1}, respectively. Together, we estimate that Ganymede loses 7.5×10^{26} neutral particles per second, or assuming a mean mass of 18 amu, approximately 23 kg/s, half that estimated for Europa.

1. Introduction

Ganymede, Jupiter's and the solar system's largest satellite, is the only known moon to possess a global, intrinsic magnetic field (Gurnett et al., 1996; Kivelson et al., 1996, 1998) and thus is a fundamentally unique type of environment, namely, a "mini-magnetosphere" embedded within the much larger Jovian magnetosphere. Ganymede's intrinsic field reaches strengths of ≈1,500 nT in the polar regions (Williams et al., 1997) and is of sufficient strength to stand off the incident Jovian plasma flow. Ganymede's magnetopause forms approximately 2.0 R_G (R_G = 2,630 km) upstream, diverting Jovian plasma around the satellite. Downstream of Ganymede, a Dungey-like cycle (Dungey, 1961) is completed as field lines are transported over the polar caps of Ganymede and reconnect, recycling the magnetic flux. The reconnection of field lines downstream of Ganymede is thought to inject particles onto bound orbits within Ganymede's magnetosphere (Williams, 2001, 2004). Previous work has simulated the plasma environment of Ganymede using single-fluid (Jia et al., 2008, 2009, 2010; Plainaki et al., 2015), Hall (Dorelli et al., 2015) and multifluid magnetohydrodynamics (MHD; Paty & Winglee, 2004, 2006; Paty et al., 2008; Payan et al., 2015), MHD/particle-in-cell (Tóth et al., 2016), and hybrid (particle ions/fluid electrons) models (Fatemi et al., 2016). Generally speaking, this ensemble of models have confirmed and elucidated our knowledge of magnetospheric dynamics at Ganymede; however, the interaction of energetic (i.e., $E > \sim 10$ keV) ions with Ganymede's magnetosphere and the precipitation of these ions onto Ganymede's surface is not yet fully understood.

The plasma interaction between Ganymede's magnetosphere and the Jovian magnetosphere controls a wide array of phenomena including surface weathering, radiolysis, and the generation of a neutral exosphere, ultraviolet aurorae, and ionospheric outflows. Ganymede possesses both polar cap/equatorial and leading/trailing hemisphere surface brightness asymmetries (Smith et al., 1979), potentially due to differential fluxes of incident charged particles to the surface (Fatemi et al., 2016; Ip et al., 1997; Khurana et al., 2007). Incident particle

radiation also leads to amorphization of crystalline water ice, in competition with thermal-induced crystallization (e.g., Famá et al., 2010; Hansen & McCord, 2004). Incident Jovian ions are known to induce radiolysis (Bahr et al., 2001; Moore et al., 2007; Teolis et al., 2006, 2017) and to sputter atomic and molecular species such as H, H_2, O, O_2, OH, and H_2O from Ganymede's icy surface (Ip et al., 1997; Johnson, 1990). The ejection of sputtered species forms a neutral exosphere about Ganymede (e.g., Barth et al., 1997; Feldman et al., 2000; Leblanc et al., 2017; Marconi, 2007; Plainaki et al., 2015; Turc et al., 2014), and in turn, Ganymede's neutral O_2 undergoes electron dissociative excitation, with subsequent emissions from atomic O at 1,304 and 1,356 Å (Eviatar, Strobel, et al., 2001; Feldman et al., 2000; Hall et al., 1998; McGrath et al., 2013; Musacchio et al., 2017). Freshly ionized ionospheric material from Ganymede has been observed by the Galileo plasma science instrument (PLS) (Frank et al., 1992) flowing outwards from the satellite (e.g., Eviatar, Vasyliunas, et al., 2001; Frank et al., 1997; Paty et al., 2008; Vasyliunas & Eviatar, 2000; Volwerk & Khurana, 2010), leading to suggestions of the possible formation of an ionized and neutral torus near Ganymede's orbit around Jupiter. Variations in the spatial structure of Ganymede's aurorae due to electromagnetic induction within the interior of the satellite may also be a window into the putative subsurface ocean of Ganymede (Saur et al., 2014). Thus, knowledge of energetic particle dynamics within Ganymede's magnetosphere is critical for understanding the surface, atmosphere, and potentially, the interior of Ganymede.

The Galileo spacecraft made repeated measurements of the energetic ion environment in the Jovian magnetosphere in general (e.g., Kane et al., 1999; Kasahara et al., 2011; Kronberg et al., 2008; Mauk et al., 2004; Radioti et al., 2005, 2007) and specifically near and within Ganymede's magnetosphere (e.g., Paranicas et al., 1999; Williams, 2001; Williams et al., 1997, 1998) using the Energetic Particle Detector (EPD; Williams et al., 1992). The EPD instrument operated during five of the six Galileo spacecraft flybys of Ganymede (G2, G7, G8, G28, and G29); a software issue prevented measurements during the initial G1 flyby. These measurements reveal a complex interaction environment for both electrons and ions. In particular, energetic ions display several features of note in the EPD data set. During crossings of Ganymede's magnetopause, the ion spectra show a loss (or significant diminishment) of convectional corotation anisotropies, indicating that Ganymede's magnetosphere significantly decelerates the incident Jovian plasma (Williams et al., 1997). Within Ganymede's magnetosphere, the ion spectra often show sharp loss cones coincident with times during which the EPD instrument viewed along the local magnetic field line (which is presumably closed to the surface of Ganymede; Williams et al., 1997, 1998). During the G28 and G29 flybys, the ion spectra revealed trapped ion distributions, notable by their relative peak in pitch angle near 90° (Williams, 2001, 2004). These trapped distributions presumably originate from the entry of Jovian ions into Ganymede's magnetosphere, most likely through the reconnection/magnetotail region downstream (i.e., on the leading hemisphere) of Ganymede. As noted by Williams (2001), a detailed modeling study is necessary to fully illuminate the various processes by which these Jovian ions become trapped onto and drift about Ganymedean field lines.

Here we present results from a particle tracing model of thermal and energetic particle dynamics in Ganymede's magnetosphere that builds upon previously published hybrid plasma simulations of Ganymede's magnetosphere (Fatemi et al., 2016). We use measured particle distributions outside of Ganymede's magnetosphere (Kivelson et al., 2004; Mauk et al., 2004) along with the electric and magnetic fields derived from the hybrid simulations of Ganymede's magnetosphere in order to appropriately calculate quantitative fluxes near and onto the surface. Furthermore, we compare our modeling results with previous work in order to highlight important similarities and differences. Section 2 describes the modeling approach used to investigate the energetic ion environment at Ganymede. Section 3 compares the model results to Galileo MAG, PLS, and EPD measurements during the Galileo G8 flyby, while sections 4 and 5 describe the thermal and energetic ion environment in near-Ganymede space and the ion precipitation to Ganymede's surface, respectively. Section 6 uses the calculated ion precipitation fluxes to quantify the flux and distribution of sputtered neutrals from Ganymede's surface. Finally, we compare our results to those of previous particle tracing models of Ganymede's environment in section 7 and conclude in section 8.

2. Model Description

Recently, Fatemi et al. (2016) presented three-dimensional, self-consistent hybrid model simulations of Ganymede's magnetospheric interaction with the Jovian magnetosphere. The hybrid model uses an extended, generalized Ohm's Law that includes the Hall term, and thus, the hybrid model captures both Hall-related and finite-Larmor radius effects. We do note that Dorelli et al. (2015) and Tóth et al. (2016) have

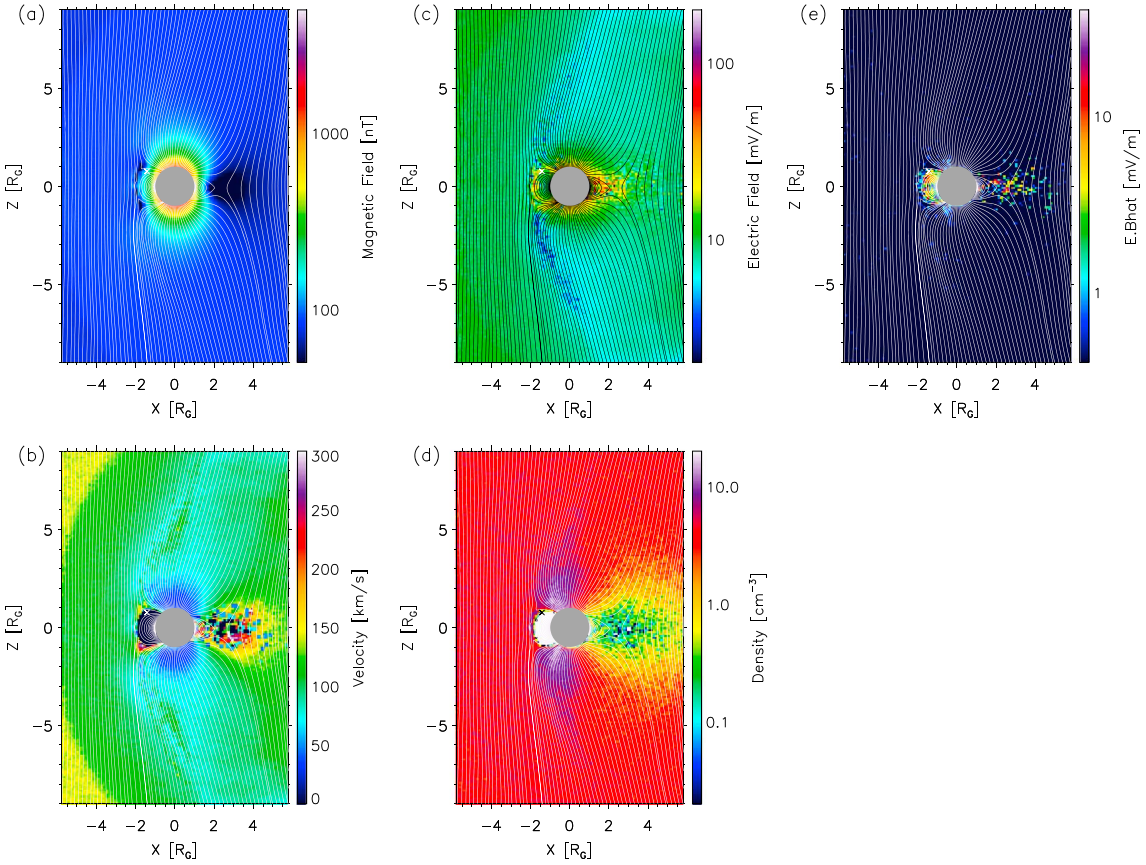

Figure 1. The magnetic and electric field magnitudes for the G8 conditions from the hybrid simulations runs of Fatemi et al. (2016). The Jovian plasma flow is from left to right. The × symbol at $[X, Z] = [-1.42, 0.76]$ R_G marks the position through which the Galileo spacecraft passed the *XZ* plane during the G8 flyby.

shown that spatial resolution of $\approx d_i/5$, where d_i is the ion inertial length, is necessary to capture some detailed aspects of the magnetopause and magnetotail reconnection at Ganymede, whereas the hybrid runs used here have lower spatial resolution of $\approx d_i/2$. Future hybrid runs may be able to achieve such high resolution; however, our current runs are at the maximum of available computing memory (which is the main limiting factor for these runs). Similar to previous modeling efforts of Ganymede's magnetosphere (e.g., Dorelli et al., 2015; Duling et al., 2014; Jia et al., 2008, 2009, 2010; Kopp & Ip, 2002; Paty & Winglee, 2004, 2006; Payan et al., 2015; Tóth et al., 2016), the hybrid results of Fatemi et al. (2016), reproduced in part here in Figure 1, show a well-developed magnetosphere around Ganymede. In particular, Figure 1 shows (a) the magnetic field magnitude, (b) the plasma velocity, (c) the electric field magnitude, (d) the plasma density, and (e) the magnitude of the electric field parallel to the magnetic field (i.e., $|\mathbf{E} \cdot \hat{\mathbf{B}}|$) for conditions similar to the G8 flyby all displayed in the XZ GPhiO plane at Y = 0, with magnetic field lines overplotted on all panels. The hybrid model results show several features, including an upstream magnetopause near 2 R_G, Alfvén wings originating from the polar regions of Ganymede, and a short magnetotail extending downstream of the satellite. Figure 1c shows that electric fields reach 100 mV/m both along the magnetopause and in the magnetotail reconnection zone with parallel electric fields, panel 1e, reaching maxima of ≈30 mV/m mainly in the upstream closed field line region and in the magnetotail.

The results of Fatemi et al. (2016) were successfully compared against Galileo magnetometer measurements taken during each of the six Galileo flybys; however, comparison to plasma and energetic particle observations were not done at that time. Nevertheless, Fatemi et al. (2016) did present model results for the precipitating flux of H^+, O^{++}, and S^{+++} ions with upstream energies between 1 and 10^4 keV by forward tracing ion trajectories through the hybrid model. Precipitating ions were shown to be mainly focused onto Ganymede's polar cap regions along open fields lines with a suppression of precipitating ion flux in the equatorial region of Ganymede along generally closed field lines. Here we extend and further explore the dynamics of thermal and energetic Jovian ions as they interact with Ganymede's magnetosphere, including their precipitation

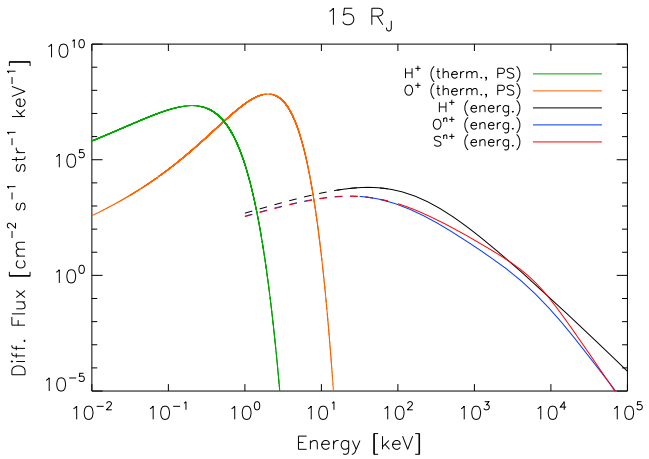

Figure 2. The differential flux distributions as a function of energy for the five ion species considered here. Thermal plasma parameters for H^+ and O^+ are taken from Kivelson et al. (2004) or Bagenal et al. (2016) and energetic particle parameters for H^+, O^{++}, and S^{+++} are taken from Mauk et al. (2004). Note that the energetic species are extrapolated down to 1 keV (shown as dashed lines).

to the surface of Ganymede. We focus solely on plasma/field conditions at Ganymede representative of the Galileo G8 flyby when Ganymede was immersed in the plasma sheet. Future work will focus on characterization of ion dynamics at Ganymede for conditions above/below the Jovian plasma sheet.

In contrast to the forward tracing approach used for energetic ion tracing in Fatemi et al. (2016), we use here a backwards Liouville tracing technique to trace ion trajectories from a given endpoint in time and space (whether on the surface of Ganymede or in near-Ganymede space) backwards through the hybrid model magnetic and electric fields. For each selected endpoint, we trace ion trajectories with discrete values of energy and angle backwards in time until the trajectory either strikes the surface of Ganymede or exits the simulation domain through one of the boundaries. Liouville's Theorem, which stipulates the conservation of phase space density along trajectories in the absence of particle collisions or other scattering processes (i.e., wave-particle interactions), allows us to then assign appropriate phase space densities to each element within the three-dimensional phase space distribution at the chosen endpoint. Particles whose back-traced trajectory intersects Ganymede are assigned zero distribution function (as Ganymede has presumably absorbed the particle at some antipodal point), while trajectories that exit the simulation domain are assigned a distribution function value based on their velocity at the simulation boundary assuming that the boundaries represent the undisturbed Jovian plasma and energetic particle distributions. We do note that ion trajectories that are traced back to the top or bottom of the simulation boundaries may in reality have distributions that are affected by the presence of the Alfvén wings propagating away from Ganymede; however, we consider this perturbation to be at most a minor discrepancy and thus proceed with the assumption of undisturbed ion distribution functions at the simulation boundaries. The backwards Liouville technique provides the advantage of high spatial and velocity space resolution of plasma distribution functions with only moderate computing requirements and has been successfully used previously at Ganymede (e.g., Allioux et al., 2013; Cooper et al., 2001) and the Moon (Fatemi et al., 2012; Poppe et al., 2017).

Knowledge of the upstream plasma and energetic ion distributions is critical for accurately modeling energetic ion dynamics in Ganymede's magnetosphere. For completeness, we ran the backwards particle tracing simulations for two separate populations: thermal and energetic, shown as differential flux in Figure 2. For the thermal distribution, we ran H^+ and O^+ with energies between 10 and 10^5 eV (e.g., Kivelson et al., 2004). For the energetic distribution, we ran H^+, O^{2+}, and S^{3+} between 10^3 and 10^7 eV (e.g., Collier & Hamilton, 1995; Keppler & Krupp, 1996; Mauk et al., 2004). We use Kivelson et al. (2004) and Bagenal et al. (2016) to define the thermal plasma parameters within the Jovian current sheet. At the radial distance of Ganymede, the current sheet plasma is assigned a total density of 4 cm^{-3}; H^+ and O^+ mass fractions of 13% and 87%, respectively (equivalent to a mean ion mass of 14 amu); a drift velocity of 140 km/s (with respect to Ganymede); and temperatures of 60 eV for protons and 200 eV for O^+. The choice of colder H^+ was motivated by comparisons to Galileo PLS observations as described below in section 3. For the energetic ions, we use the distributions reported by Mauk et al. (2004) within the Jovian plasma sheet at a distance of 25.0 R_J (the "G8_PS/A" column in Table 1 of Mauk et al., 2004) scaled up in intensity by a factor of 5 to approximate the conditions at 15 R_J within the plasma sheet (see Figure 3(a) of Mauk et al., 2004). The energetic distributions are described as the combination of a kappa distribution with a break to softer spectra at higher energies. Note that the energetic distributions were only reported down to varying energies between 10 and 100 keV in Mauk et al. (2004); thus, we extend the functional forms for energetic species down to 1 keV (dashed portion of curves in Figure 2). The integrations for each particle are conducted by a fourth-order Runge-Kutta algorithm with timestep, $dt = 10^{-3}\Omega_g^{-1}$, where Ω_g is the local gyrofrequency.

3. Comparison to Galileo Measurements

Before applying the particle tracing model to computation of the ion flux to Ganymede's surface, we have first compared the modeled particle fluxes along the Galileo G8 trajectory to those measured by the Galileo

plasma instrumentation (PLS; Frank et al., 1992) and EPD (Williams et al., 1992). The Galileo spacecraft executed the G8 flyby of Ganymede on 7 May 1997 at a minimum altitude above the surface of 1,599 km. The Galileo spacecraft trajectory passed by the upstream (or trailing) hemisphere of Ganymede approximately 0.5 Ganymede radii above Ganymede's equatorial plane, passing into the closed field line region of Ganymede's magnetosphere. At the time of the G8 flyby, Ganymede was immersed inside the Jovian plasma sheet. More detailed discussions of the G8 flyby can be found in several previous works (e.g., Eviatar et al., 2000; Kivelson et al., 1998, 2002; Williams et al., 1998).

The Galileo PLS instrument is a hemispherical electrostatic analyzer that measured the ion and electron distributions between energy-per-charges of ∼0.9 eV to ∼50 keV (Frank et al., 1992). Coverage of approximately 80% of the sky is enabled by orientation perpendicular to the spin axis of the Galileo spacecraft. The PLS instrument can operate in several different modes that possess different time, energy, and angle resolution, the details of which are presented in, for example, Appendix A of Bagenal et al. (2016). We used the GO-J-PLS-3-RDR-FULLRES-V1.0 data set available from NASA's Planetary Data System, which provides ion count rates at approximately spin phase resolution (i.e., 20 s) for all seven PLS anodes. Following the discussion in Appendix A and the supplemental information of Bagenal et al. (2016), we selected only PLS data for mode 2, which consists of observations at every fourth PLS energy step, ranging between energies of approximately 20 eV to 30 keV. We interpolated linearly over energy bins with no measurements as well as over periods during which PLS was observing in mode 1. Finally, the count rates were transformed to differential energy flux by applying the individual geometric factors for each anode as listed in Bagenal et al. (2016). We do not apply any background subtraction of counts.

The Galileo EPD observations used here for comparison to the energetic particle tracing model include data from the Low Energy Magnetospheric Measurement System (LEMMS) and the Composition Measurement System (CMS; Williams et al., 1992). From the LEMMS data set, we have used the "A" channel, which detects ions with $Z \geq 1$ in eight energy bins spanning 22 keV to 3.2 MeV. From CMS, we have used the "TP," "TO," and "TS" channels, which record H^+, O^{n+}, and S^{n+} ions, respectively, in three ("TP1 – TP3"), four ("TO1 – TO4"), and three ("TS1 – TS3") energy bins, respectively. The TP channels measure protons with energies between 80 keV and 1.14 MeV, the TO channels measure oxygen energies between 192 keV and 9 MeV, and the TS channels measure sulfur energies between 512 keV and 9.92 MeV. In addition to identifying the correct channels as a function of energy and mass, one must also accurately take into account the EPD instrument pointing during its flyby past Ganymede. The EPD instrument was mounted on the spinning portion of the Galileo spacecraft and also employed an additional rotating platform for instrument pointing. The Galileo spin axis and the EPD motor spin axis were oriented orthogonally such that the EPD instrument could measure a full 4π particle distribution every seven spacecraft spin periods (∼140 s). The instantaneous field of view of the EPD LEMMS and EPD CMS detectors consisted of cones with opening angles of 15° and 18°, respectively. The EPD pointing information during the G8 flyby was downloaded from the NASA Planetary Data System and converted to GphiO coordinates using SPICE frame transformation routines. At each EPD measurement time, we used the corresponding instrument pointing vector and field of view to mask the full three-dimensional velocity distribution generated by the particle tracing model.

Figure 3 provides an overview of the Galileo MAG, PLS, and EPD observations taken during the G8 flyby. Panel 3a shows the magnetometer measurements, with the Jovian magnetic field dominant before and after the closest approach at strong, negative B_z values and the passage through Ganymede's magnetosphere between approximately 15:50 and 16:05 UTC. Closest approach to Ganymede occurred at approximately 15:57 UTC, as shown by the Galileo spacecraft position in GPhiO coordinates and distance from Ganymede in panels 3b and 3c, respectively. Panel 3d shows the spin-averaged PLS ion spectra, while panels 3e – 3h show the EPD A, TP, TO, and TS channel observations, respectively. The PLS data show the presence of two separate populations of ions outside of Ganymede's magnetosphere at approximate energies of 0.5 and ≈8 keV, corresponding to the corotating H^+ and O^+ populations, respectively. PLS ion spectra after passage through Ganymede's magnetosphere are slightly higher in magnitude, indicating a relative increase in density over the conditions before entry into Ganymede's magnetosphere. The PLS spectra show bursts of increased flux near energies of 5 – 10 keV near the magnetopause crossings (specifically, near 15:52 – 15:53 and 16:00 – 16:03) with a broad, general decrease in fluxes over all energies deepest within Ganymede's magnetosphere. As reported previously (Williams et al., 1998), notable features in the G8 EPD ion spectra include signatures of convective anisotropy outside of Ganymede's magnetosphere, a general decrease of convective anisotropies within Ganymede's magnetosphere, and periodic decreases in the ion flux during brief intervals within Ganymede's

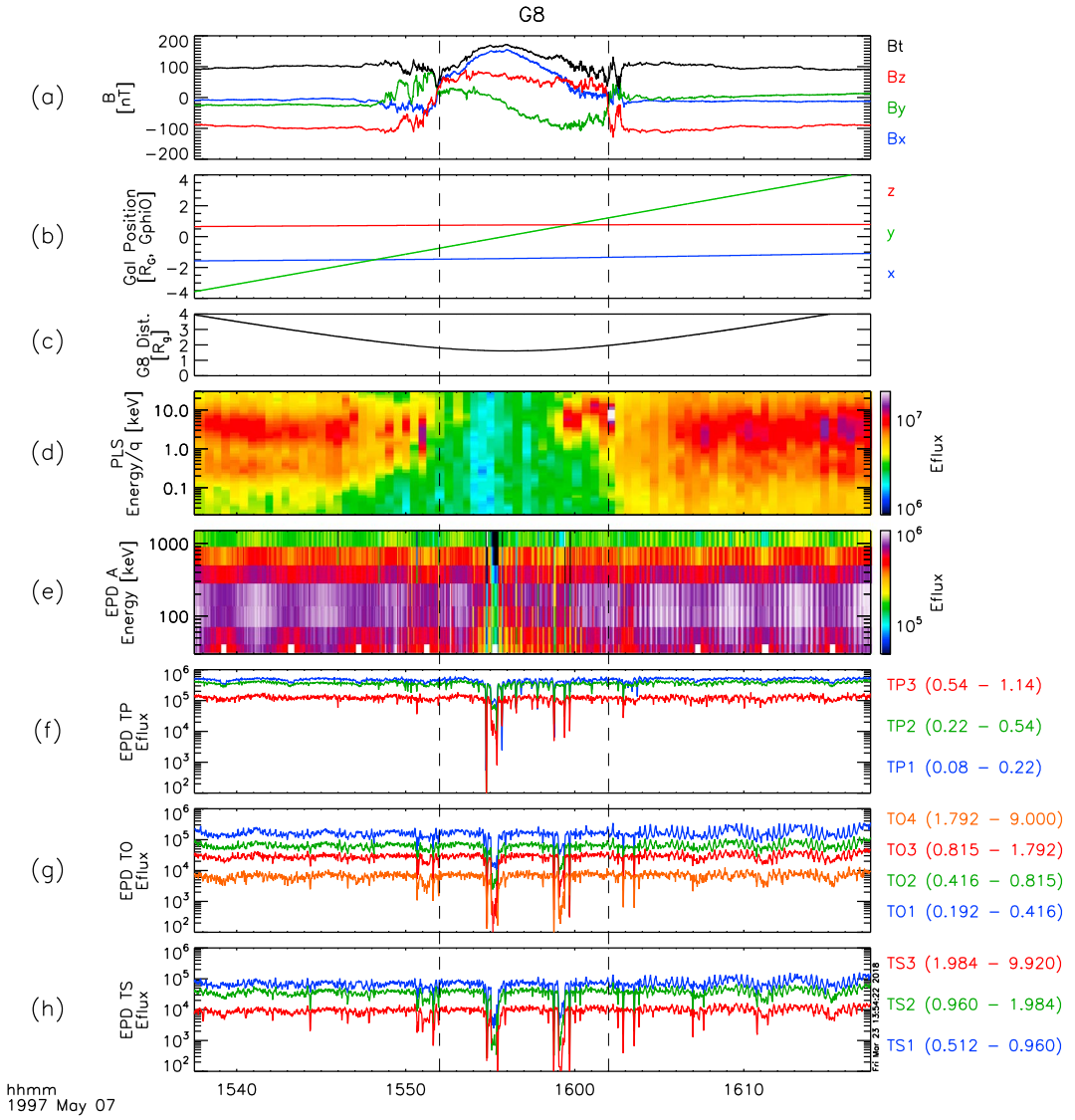

Figure 3. An overview of the Galileo observations during the G8 flyby: (a) magnetic field; (b) Galileo position in GPhiO coordinates; (c) Galileo distance from Ganymede; (d) PLS ion spectra; (e) EPD A channel spectra; and (f–h) EPD TP, TO, and TS channel data, respectively. All differential energy fluxes ("Eflux") are in units of keV/cm^2/s/str/keV and energy ranges listed for the TP, TO, and TS channels are in MeV. Vertical dashed lines mark the magnetopause crossings as identified in Kivelson et al. (1998; Table 2).

magnetosphere. The convective anisotropy signature is visible in the EPD spectra shown in panels 3e–3h as periodic modulations before and after passage through Ganymede's magnetosphere. The dropouts in the EPD ion fluxes occur both as longer period (~30 s) and shorter period (~5 s) events.

Figure 4 shows a comparison of Galileo MAG and PLS data to modeled observations of the magnetic field and ion spectra for the G8 flyby. We note that Fatemi et al. (2016) previously presented comparisons between the Galileo MAG data and hybrid model simulations of Ganymede's magnetosphere during each of the six Ganymede flybys with positive agreement. The Galileo MAG and model-derived magnetic fields are shown here in panels 4a and 4b, respectively. The hybrid magnetic fields capture many of the observed MAG features, including the strong compression in B_x, the sinusoidal variation of B_y, and the reversal of sign in B_z. Additionally, the modeled magnetic field magnitude captures local minima near both of the magnetopause crossings, in agreement with the MAG observations. One discrepancy of note, as discussed also in Fatemi et al. (2016), is the somewhat larger magnetosphere in the model as opposed to the data, especially, for example, as seen in the B_y and B_z components at the magnetospheric exit. This discrepancy is due to the lack of energetic

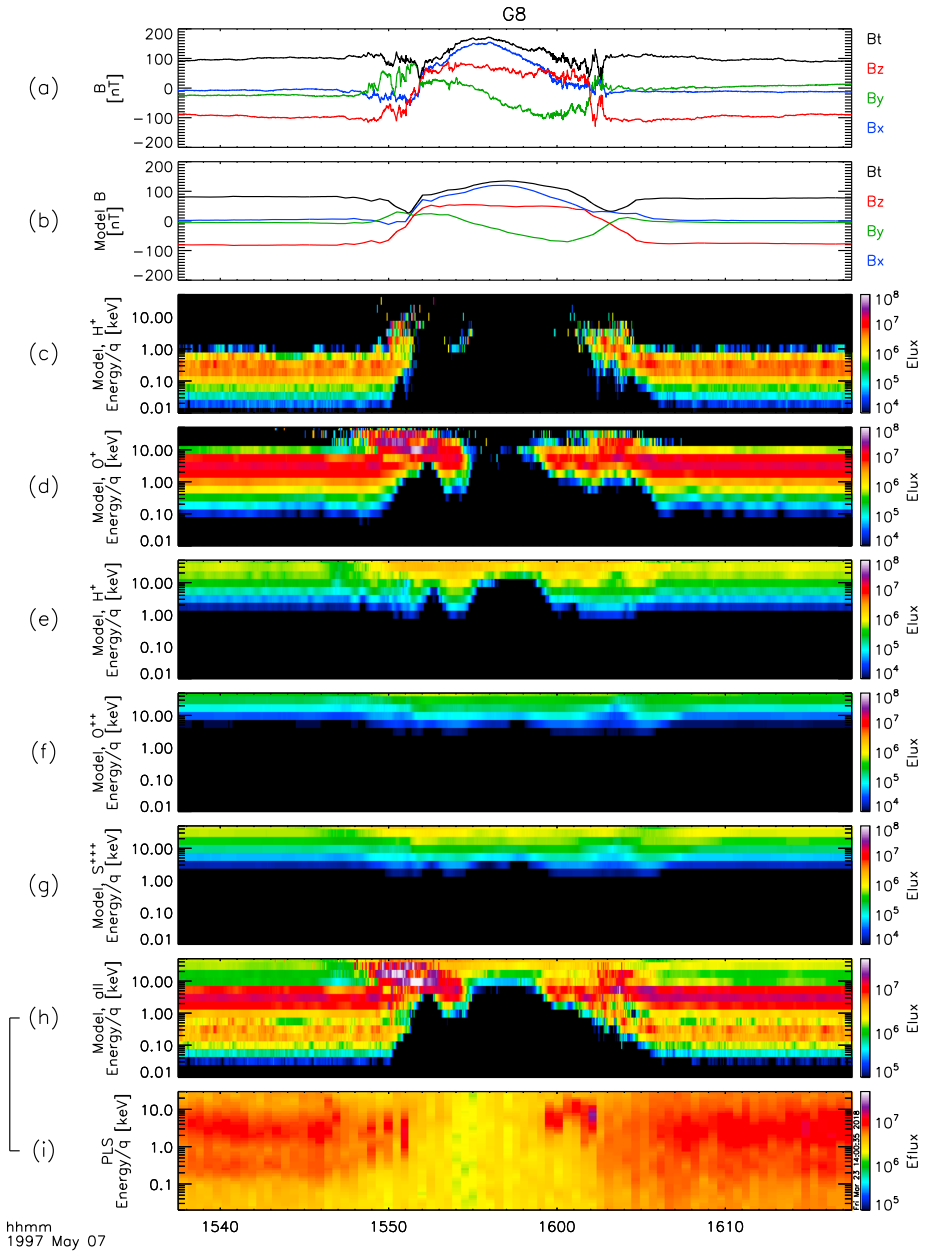

Figure 4. A comparison between the Galileo MAG and PLS observations and the modeled magnetic field and ion spectra. Panels (a) and (b) compare the Galileo and model magnetometer measurements, respectively. Panels (c)–(g) show the thermal H^+, thermal O^+, energetic H^+, energetic O^{++}, and energetic S^{+++} contributions to the modeled ion spectra, respectively. Panels (h) and (i) compare the total modeled ion spectra and the PLS observations, respectively. Note that panel (i) has a different color range than that first presented in Figure 3d. All differential energy fluxes ("Eflux") are in units of keV/cm^2/s/str/keV.

(>10 keV) ions in the hybrid model, which carry a significant amount of pressure relative to the thermal ions (e.g., Mauk et al., 2004) and thus tend to compress Ganymede's magnetosphere to a greater degree than captured with the hybrid model.

The next five panels of Figure 4 show the contributions from each individual modeled ion specie as would be observed by the PLS instrument, including (c) thermal H^+, (d) thermal O^+, (e) energetic H^+, (f) energetic O^{++}, and (g) energetic S^{+++}. Note that the observed energies of the multiply-charged species (O^{++} and S^{+++}) have been appropriately scaled down in order to take into account the fact that the PLS instrument measures energy per charge. Both thermal species, panels 4c and 4d, have relatively narrow energy spectra outside

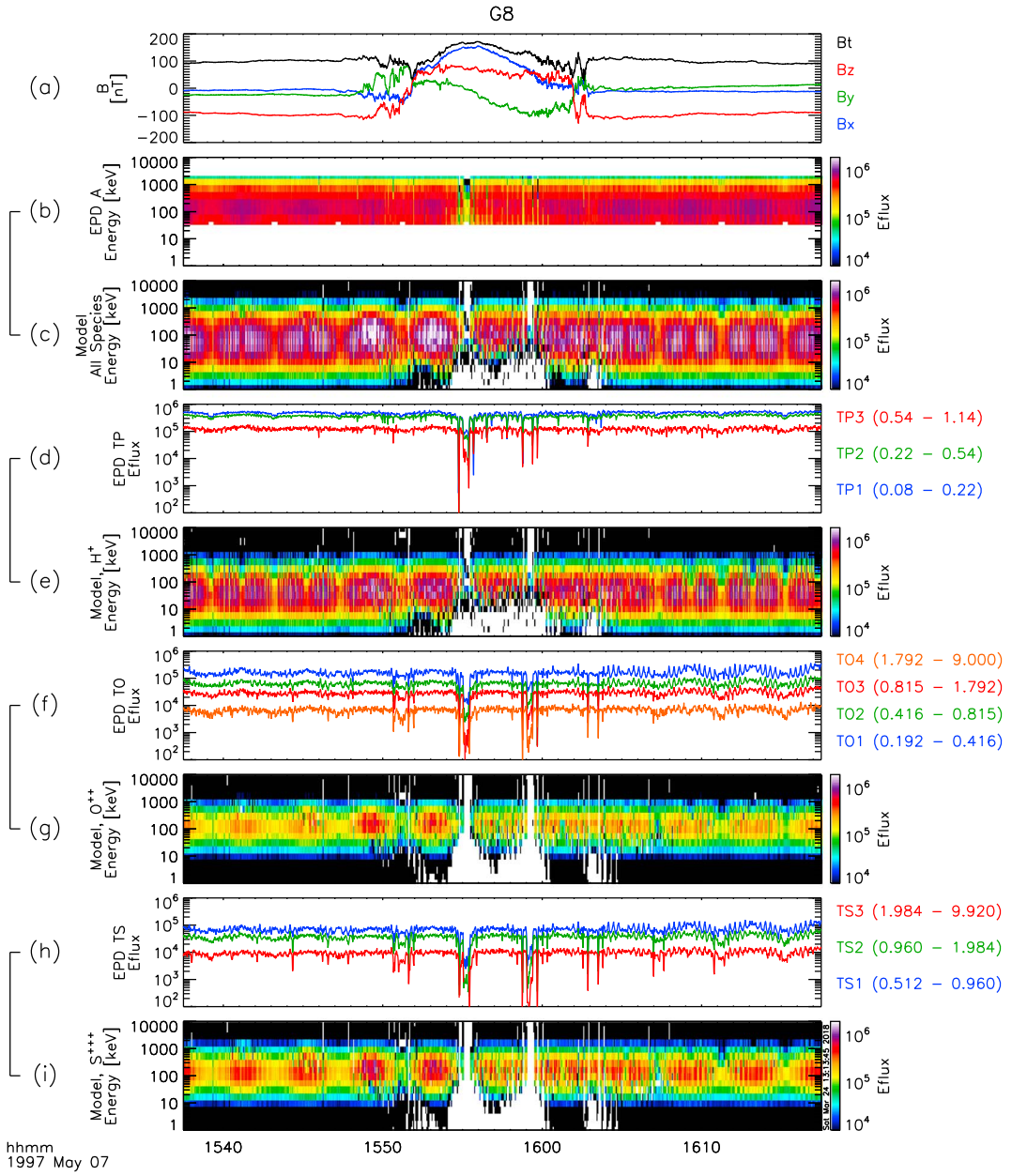

Figure 5. A comparison of Galileo EPD measurements and energetic ion model results for the G8 flyby. Panels include (a) the magnetic field as observed by Galileo MAG, (b) the Galileo spacecraft distance from the center of Ganymede, (c) the model H^+ differential energy flux, (d) the Galileo EPD A channel measurements, (e) the model O^{++} differential energy flux, (f) the Galileo EPD TO channel measurements, (g) the model S^{+++} differential energy flux, and (h) the Galileo EPD TS channel measurements. Energy ranges listed for the TP, TO, and TS channels are in MeV. EPD = Energetic Particle Detector.

of Ganymede's magnetosphere in the corotating Jovian flow, with thermal H^+ fluxes peaking at energies of 0.5 keV and thermal O^+ fluxes peaking at energies of 3–5 keV. Both thermal species show the presence of accelerated ions near the flanks of Ganymede's magnetosphere, with thermal H^+ accelerated up to 10 keV and thermal O^+ accelerated up to nearly 30 keV. Deep within Ganymede's magnetosphere, the fluxes for both thermal species completely drop out, with thermal O^+ penetrating slightly deeper into Ganymede's magnetosphere than thermal H^+. The energetic species, meanwhile, shown in panels 4d–4f, appear at energies greater than approximately 5 keV throughout the passage through Ganymede's magnetosphere. Energetic H^+ shows an increase in fluxes above 20 keV with occasional depletions in flux below 10 keV during periods within Ganymede's magnetosphere (15:48–16:02 UT). Energetic O^{++} and S^{+++} show only slight variations

in flux within Ganymede's magnetosphere. Panel 4h shows the total modeled ion spectra for PLS, summing over all five individual ion species present in the model. Both the thermal populations are readily identified with additional contributions evident from the energetic populations. In comparison, the modeled ion spectra capture several of the features in the Galileo PLS observations, including the double-peaked spectra as a function of energy due to the presence of both thermal H^+ and O^+, the drop in fluxes when passing through Ganymede's magnetosphere (approximately 15:50–16:03 UT), and the acceleration of ions near both magnetopause crossings (at 15:50–15:52 UT and 16:00–16:03 UT). The modeled ion spectra do show a larger time period of depleted ion fluxes than does the PLS spectra, due to the wider modeled magnetosphere discussed above.

Figure 5 compares the Galileo EPD measurements with modeled energetic ion spectra. Panel 5a again shows the Galileo MAG observations for reference. The subsequent four pairs of panels compare ion spectra from (b–c) the EPD A channel and the sum of all modeled ion species, (d–e) the EPD TP channel and energetic H^+ only, (f–g) the EPD TO channel and energetic O^{++} only, and (h–i) the EPD TS channel and energetic S^{+++} only. The modeled spectra appropriately capture all of the features in the EPD observations discussed previously. Convective flow anisotropy features are seen in all three modeled ion spectra both before and after the magnetospheric passage as periodic variations in the differential ion flux. Between approximately 15:50 and 16:05, the model spectra in all three species show a dropout in fluxes for energy channels typically less than 10 keV with a pair of nearly complete dropouts over all energies at approximately 15:55 and 15:59. These drops in the modeled flux (discussed in further detail in the next paragraph) correspond well with the Galileo EPD measurements in the A, TP, TO, and TS channels and also correspond with the passage of the Galileo spacecraft through Ganymede's magnetosphere (i.e., magnetopause entry and exit crossings were identified at approximately 15:53 UT and 16:03 UT, respectively; Kivelson et al., 1998; Williams et al., 1998). The model also captures the much shorter duration dropout spikes seen in the EPD data set, including, for example, those at 15:50:39, 15:54:46, 15:58:46, 16:02:53, and 16:03:31 UT (among others). We do note that the model overpredicts the depth of energetic particle dropouts in the A and TP channels at 15:59 UT. This could potentially be due to time-varying fields and particle populations due to the proximity to Ganymede's magnetopause; such time-variable effects would not be captured in the hybrid due to the steady-state upstream conditions in the model. Nevertheless, the overall comparison between the modeled and observed energetic ion spectra is successful.

Figure 6 shows a more detailed comparison of the EPD spectra and the ion tracing model. Specifically, we focus on a shorter interval of time between 1999-05-07/15:54:00 and 15:56:30 UT as the Galileo spacecraft passed through closest approach at 15:56:09 UT. Panels 6a and 6b show the EPD A channel spectra and the total modeled ion spectra for the entire G8 flyby time period (i.e., that shown in Figure 5), while panels 6c–6g show data within the time period of 15:54 to 15:56:30. The EPD instrument recorded several features of note during this time interval including sharp dropouts at 15:54:46, 15:55:24, and 15:55:42 UT and a broader, energy-dependent drop in fluxes between 15:55:02 and 15:55:21. Williams et al. (1998) noted that drops in the EPD counting rate corresponded with times when the instrument looked along the local magnetic field line while in Ganymede's magnetosphere. These field lines are presumably closed and thus should be void of particles due to absorption by Ganymede itself. Observations at time 15:54:46 represent such an event with the EPD pointing along a pitch angle of $\approx 20°$. To confirm this, we traced ions over a range of energies from the position of the Galileo probe at 15:54:46 backwards in time, with initial conditions corresponding to the observational geometry of the EPD detector. Panels 6h and 6i show H^+ trajectories in the GPhiO XY and XZ planes, respectively, for this time period. Trajectories at all energies start from the Galileo probe position of [−1.43, −0.2, 0.75] R_G and all map back to approximately the same position on the northern hemisphere of Ganymede. Thus, as these trajectories were traced *backwards* in time, their intersection with Ganymede implies that such trajectories have no phase space density; in other words, these hypothetical trajectories correspond to particles that were absorbed elsewhere on Ganymede before being able to reach EPD.

In contrast to the observations at 15:54:46, observations between 15:55:02 and 15:55:20 show residual fluxes mainly in the lower A channel energies, despite EPD pointing at pitch angles of 45° or less. The corresponding modeled ion fluxes, panel 6g, also show such an effect. We repeated the backwards tracing exercise from the position and positing of Galileo at 15:55:19, the results of which are shown spatially in panels 6j and 6k. Here the particle trajectories over all energies are much more complex and do not all simply intersect the surface of Ganymede, despite looking along a fairly field-aligned direction within Ganymede's magnetosphere (i.e., along closed field lines that intersect Ganymede's surface). The lowest energy ion at 30 keV

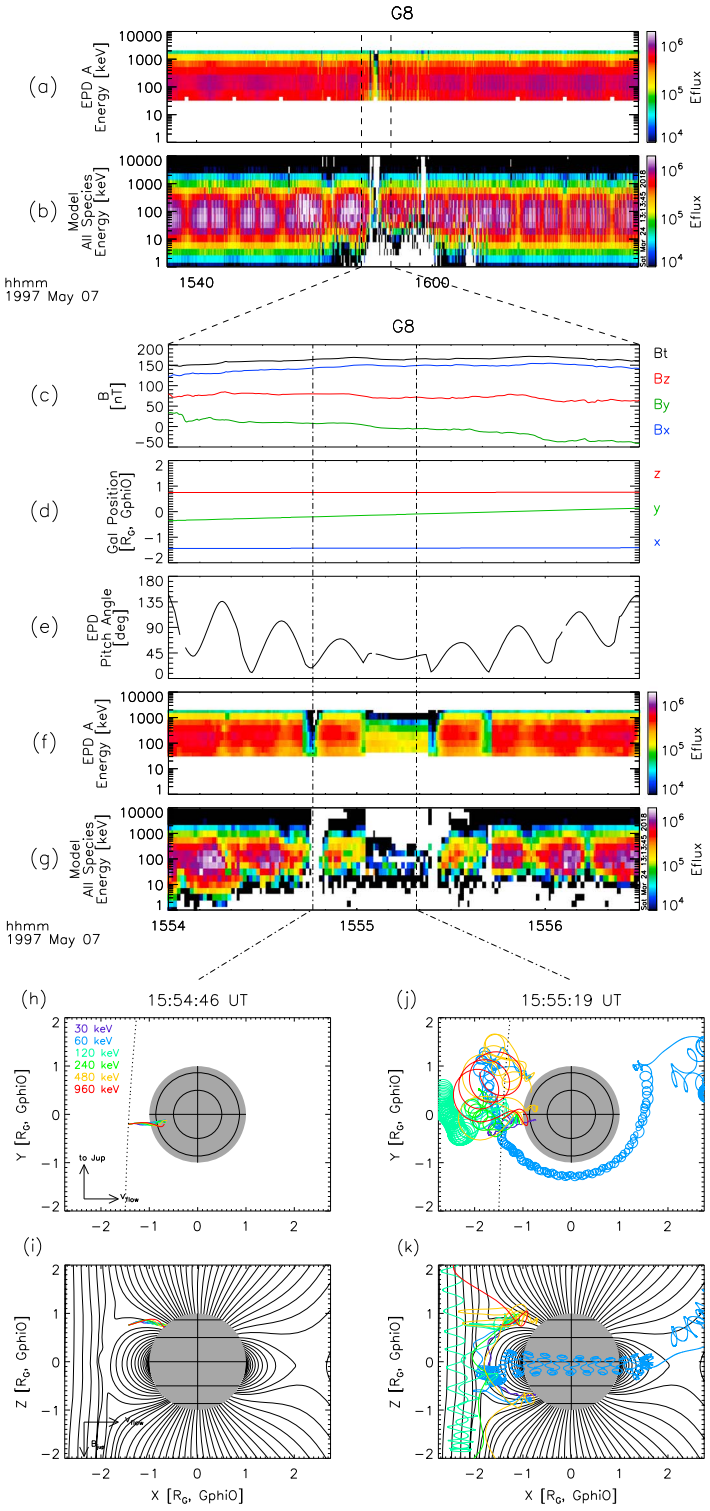

Figure 6. Panels (a) and (b) show the Galileo EPD A spectra and model spectra for the full G8 flyby period (i.e., that shown in Figure 5). A detailed comparison of Galileo measurements and model fluxes is shown between 1999-05-07 15:54 and 15:56:30 UT including (c) the magnetic field as observed by Galileo MAG, (d) the Galileo spacecraft position in GPhiO coordinates, (e) the pitch angle as observed by Galileo EPD, (f) the Galileo EPD A channel measurements, and (g) the modeled total differential ion energy flux. (h–k) Samples of backwards-traced H^+ trajectories at six energies for two different times, 15:54:46 UT and 15:55:19 UT (noted as dashed lines on the left panel, respectively), in both the XY and XZ GPhiO planes. The dotted lines in panels (h) and (j) denote the Galileo spacecraft trajectory for the G8 flyby. EPD = Energetic Particle Detector.

(purple trace) follows the Ganymede field line southwards and does intersect Ganymede's surface near −45° latitude. This corresponds with a dropout in the EPD A0 channel (measuring energies of 22–44 keV) at this time. At 60 keV (blue), backwards tracing shows first a mirror point in the southern hemisphere of Ganymede, followed by evolution along a trapped trajectory that undergoes bounce and drift motion around Ganymede. The 60-keV particle drift around Ganymede continues from the upstream hemisphere, around the anti-Jovian hemisphere, and finally to the downstream hemisphere of Ganymede. At approximately 60° W longitude, the trajectory passes through Ganymede's magnetotail region and drifts up the Jovian field line out of the +Z end of the simulation domain. This trapped trajectory is an example of a class of ion trajectories that comprise Ganymede's ionic radiation belts, as observed previously by Galileo EPD (Williams, 2001, 2004). Indeed, these simulations support the hypothesis put forward by Williams (2001) that Ganymede's ionic radiation belts are supplied by ions that are injected into Ganymede's magnetosphere through its magnetotail. The remaining four ion trajectories at energies of 120, 240, 480, and 960 keV all have similar types of trajectories including high-latitude mirror bounce points (specifically, see the 480-keV [yellow] trajectory in both the northern and southern hemispheres) and quasi-chaotic, nonadiabatic trajectories that intersect Ganymede's magnetopause (e.g., see also Chen & Palmadesso, 1986; Martin, 1986; Speiser, 1965). We emphasize here that just because an ion trajectory successfully exited Ganymede's magnetosphere during backwards tracing does not imply that such a trajectory carries a significant phase space density. By inspecting Figure 6g at the 15:55:19 UT time (right-most vertical dashed line), one can see that the modeled H^+ flux is zero for energies greater than approximately 200 keV in approximate agreement with the Galileo EPD A channel measurements, shown in Figure 6f. Thus, the successful comparison of the energetic particle tracing model results with the Galileo EPD measurements during the G8 flyby validates our modeling approach and allows us to use the energetic particle tracing model to further explore energetic ion dynamics in Ganymede's magnetosphere.

4. Energetic Ion Environment in Near-Ganymede Space

The backwards ion tracing model can be used to define the energetic ion population characteristics in near-Ganymede space, both within and outside of Ganymede's magnetosphere. To do so, we traced trajectories for the full three-dimensional ion velocity distribution for all three energetic species, H^+, O^{++}, and S^{+++}, at three discrete energies, 30 keV, 300 keV, and 3 MeV in two spatial planes, the XZ GPhiO plane at Y = 0 and the XY GPhiO plane at Z = 0. We used a spatial resolution of 0.1×0.1 R_G in both planes. Figures 7 and 8 show the ion flux for each individual ion species and energy, normalized to the average upstream flux at the simulation boundary (X = −6 R_G), for the XZ and XY planes, respectively. Several noteworthy features are readily apparent in both planes.

In the XZ GPhiO plane, Figure 7, dominant features include (1) a shielded region on the upstream side of Ganymede's magnetosphere extending out to $X \approx -2.0$ R_G, (2) enhancements extending vertically along the upstream boundaries of the Alfvén wings, (3) relative deficits in the flux immediately over the polar caps of Ganymede, (4) evidence of quasi-trapped ion populations and relative enhancements over the undisturbed upstream flux on the leading (downstream hemisphere) of Ganymede at low latitudes (especially notable in 30 keV H^+, and 300 keV H^+, O^{++}, and S^{+++}), (5) deficits in ion flux extending from the polar caps and leading (downstream) hemisphere of Ganymede that extend vertically up the downstream boundaries of the Alfvén wings, and (6) an enhancement in the ion flux downstream of the reconnection region of Ganymede's magnetotail, especially notable in the 30-keV H^+, and 300 keV H^+, O^{++}, and S^{+++} fluxes. Feature (1) is an expected feature in the energetic ion flux due to the higher magnetic field strength and subsequent shielding within Ganymede's magnetosphere, discussed above in section 3 with respect to Galileo EPD comparisons and as discussed in numerous prior publications (e.g., Cooper et al., 2001; Khurana et al., 2007; Williams, 2001; Williams et al., 1998). As is expected, the shielded region shrinks in size upstream of Ganymede as a function of increasing particle energy (which, in turn, determines the particle gyroradius). Feature (2), namely, the enhancements in flux along the upstream Alfvén wing boundaries, is caused by both deceleration of the incident plasma upon entering the Alfvén wings and by the deflection of incident trajectories from the near-equatorial plane up and over the closed field lines region of Ganymede's magnetosphere upon interaction with Ganymede's upstream magnetopause fields. Deficits in the ion flux over Ganymede's polar caps, feature (3), are mainly caused by particle shadowing by the solid surface of Ganymede, accessible through the open field lines in the polar region. Quasi-trapped distributions in the ion flux, feature (4), are seen in the 30-keV H^+ and 300-keV H^+, O^{++}, and S^{+++} distributions just downstream of Ganymede. These distributions trace out the distorted, closed field line region in Ganymede's leading, equatorial hemisphere as particles bounce between near-surface

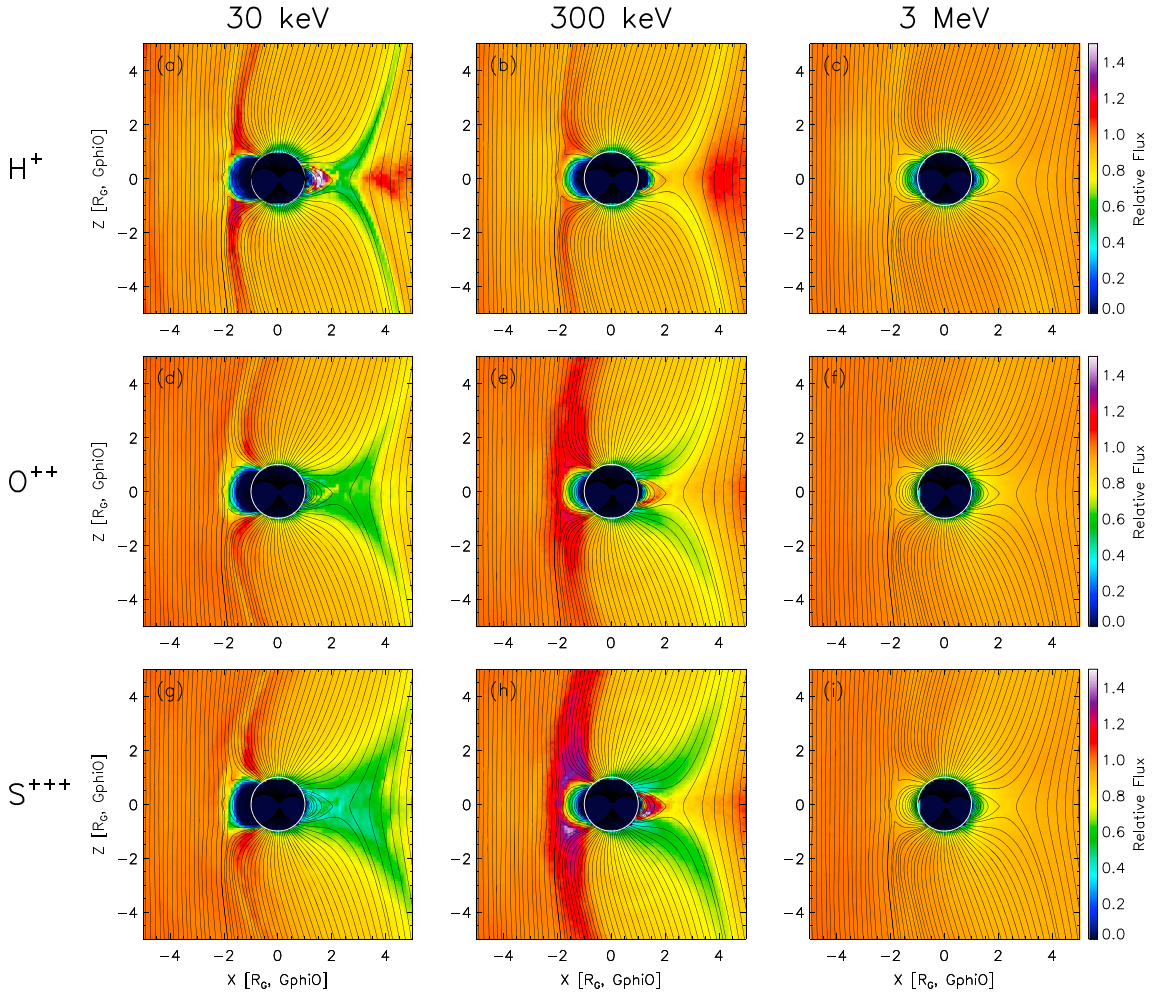

Figure 7. Fluxes of energetic ions in near-Ganymede space, shown in the GPhiO XZ plane. Each panel is individually normalized to the average upstream flux at $X = -5$ R_G. Incident Jovian plasma flow is from left to right, and magnetic field lines are overplotted.

mirror points while also drifting longitudinally around Ganymede (e.g., see Figures 6j and 6k and the discussion below of Figure 8). These trapped ion populations support the Ganymedean ionic radiation belt observations of Williams (2001). Feature (5), namely, the region of deficits in the energetic ion fluxes that extend generally along the downstream boundaries of the Alfvén wings, are caused by both the reacceleration of field lines once they disconnect from Ganymede's magnetosphere and some loss of ions from the flux tubes to the reconnection region of Ganymede's magnetotail. Finally, the enhancement of energetic ion fluxes downstream of Ganymede ($x > \sim 3$ R_G) is due to the expulsion and reacceleration of plasma from reconnection in Ganymede's magnetotail (e.g., Fatemi et al., 2016; Jia et al., 2009).

In the XY GPhiO plane, Figure 8, dominant features include (1) a general decrease in the energetic ion flux from the upstream boundary (i.e., near $X = -5$ R_G) approaching Ganymede's magnetosphere; (2) a shielded region with almost no energetic ion flux within approximately 2.0 R_G mainly on the upstream and Jovian-facing sides of Ganymede; (3) enhancements in the energetic ion flux on the downstream, slightly anti-Jovian side of Ganymede within 2.0 R_G (mainly visible in 30-keV H^+, and 300-keV O^{++} and S^{+++}); and (4) enhancements in the energetic ion flux downstream of Ganymede within the magnetotail (mainly visible in 30-keV H^+ and all species at 300 keV). These features correspond to several of the features in the XZ GPhiO plane discussed in the previous paragraph. The 3-MeV ion flux distributions for all three species show only mild depressions in flux nearest Ganymede's surface, with typical fluxes relative to upstream of ≈0.5 at Ganymede's surface. This factor of two decrease is approximately just that caused solely by the solid object shadowing by Ganymede, regardless of the role of electric and magnetic fields in Ganymede's magnetosphere.

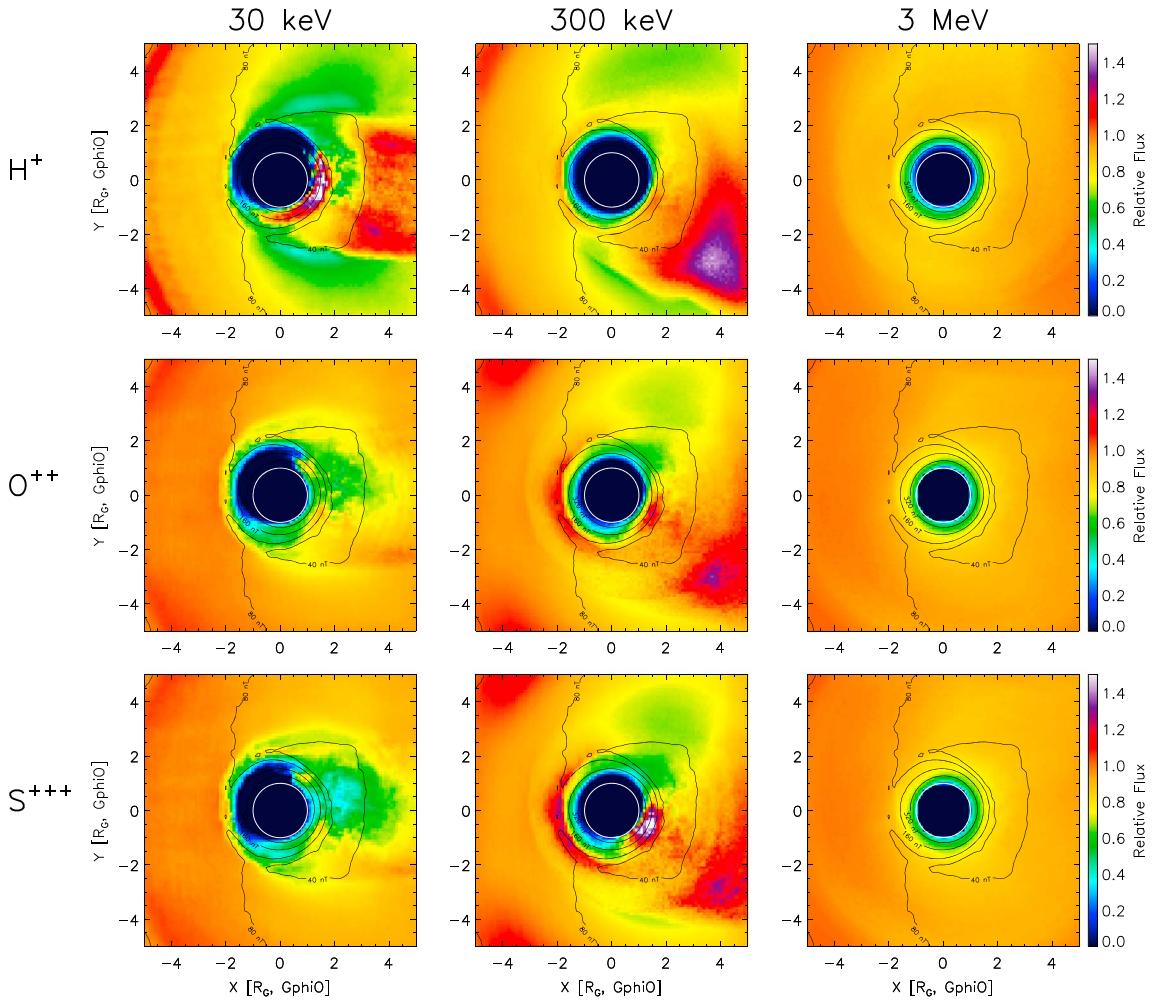

Figure 8. Fluxes of energetic ions in near-Ganymede space, shown in the GPhiO XY plane, shown in the same manner as Figure 7. Contours of magnetic field strength are overplotted on all panels.

5. Thermal and Energetic Ion Fluxes to Ganymede's Surface

Having calculated the energetic ion flux in near-Ganymede space, we now proceed to calculate the precipitating ion flux to the surface of Ganymede. As discussed in section 1, the incident ion flux controls the weathering of the surface of Ganymede (e.g., Hansen & McCord, 2004; Khurana et al., 2007), the production of radiolytic species in the upper surface layers (e.g., Cooper et al., 2001; Gomis et al., 2004; Moore et al., 2007; Teolis et al., 2017), and the production of a sputtered neutral exosphere about Ganymede (e.g., Hall et al., 1998; Marconi, 2007; Plainaki et al., 2015; Turc et al., 2014). We use the same backwards Liouville tracing technique as discussed in section 2 to construct full three-dimensional ion phase space distributions on the surface of Ganymede with 1° × 1° resolution in latitude and longitude. While sections 3 and 4 primarily focused on the energetic ion species, we present here both the thermal and energetic ion populations as both play an important role here with regard to precipitation onto and weathering of Ganymede's surface.

We first present in Figure 9 the ion flux to the surface of Ganymede separated by the five particle species in our model: (a) thermal H^+, (b) thermal O^+, (c) energetic H^+, (d) energetic O^{++}, and (e) energetic S^{+++}. All panels are normalized to identical color scales and oriented such that the sub-Jovian point is at 0°/360° and the leading (downstream) and trailing (upstream) hemispheres are centered on 90° and 270°, respectively. For thermal protons, panel (a), the flux in the trailing hemisphere (180° – 360°) is concentrated in the polar regions of Ganymede, with essentially no flux reaching the surface at latitudes less than 30°. The peak thermal H^+ flux occurs on the trailing hemisphere along two narrow bands at latitudes ranging from 40° to 70° latitudes in both the northern and southern hemispheres. These narrow bands correspond to the open-closed field

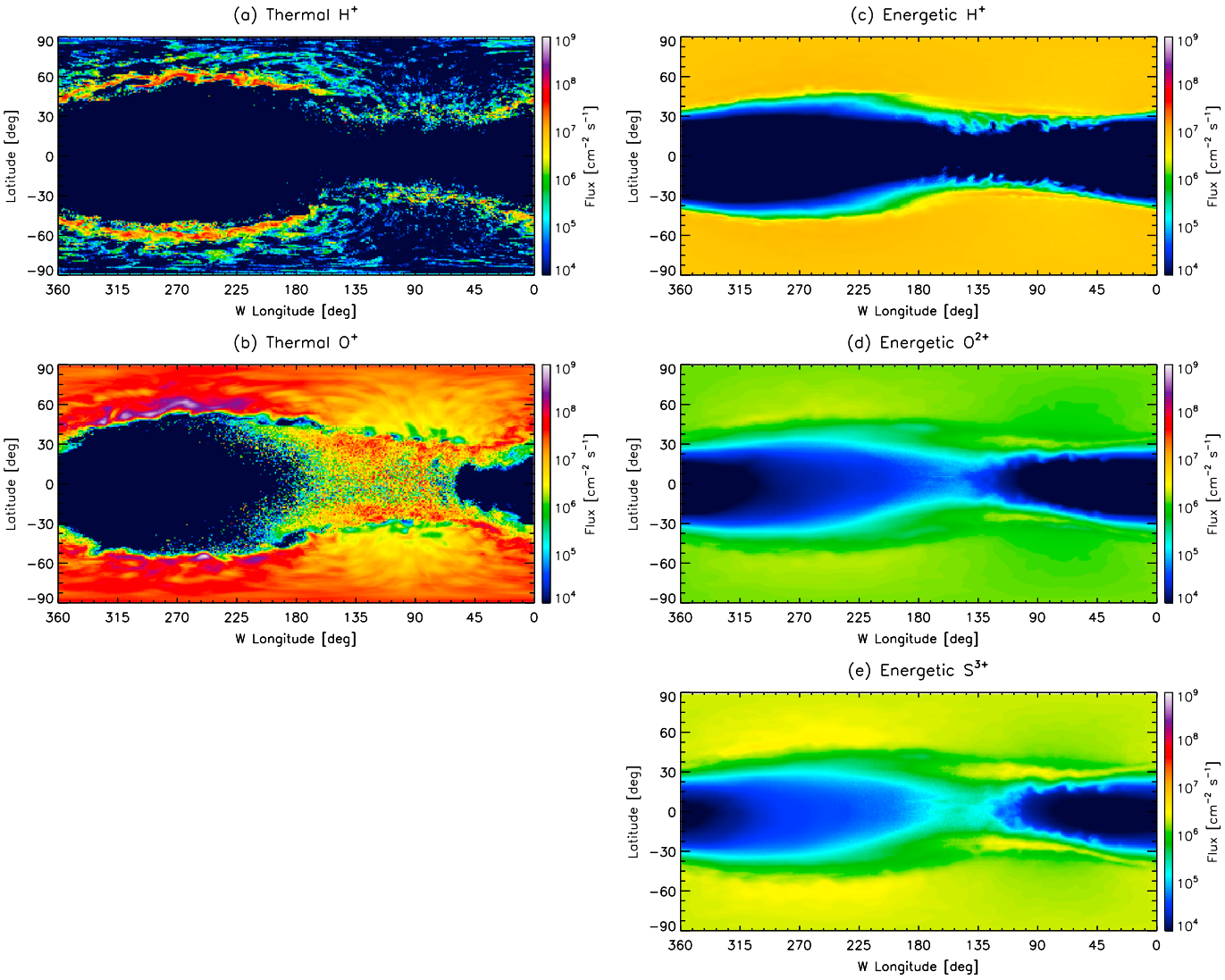

Figure 9. The flux ions to the surface of Ganymede separated by upstream distribution and type, including (a) thermal H^+, (b) thermal O^+, (c) energetic H^+, (d) energetic O^{++}, and (e) energetic S^{+++}. The leading (downstream) hemisphere of Ganymede is between 0° and 180° W longitude and the trailing (upstream) hemisphere of Ganymede is between 180° and 360°.

line boundaries on Ganymede's trailing hemisphere (compare to, e.g., Jia et al., 2008, Figure 6, and Fatemi et al., 2016, Figure 1). Thermal plasma incident on the upstream, closed-field line portion of Ganymede's magnetosphere is diverted around the magnetosphere and precipitates onto Ganymede through the magnetic cusp region (i.e., the open-closed field line boundary). The thermal O^+ fluxes to Ganymede's surface are much broader and of much higher values than thermal H^+, covering the polar cap regions of Ganymede nearly uniformly. Similar to thermal H^+, the peak O^+ flux to the surface is along the open-closed field line boundaries on the trailing hemisphere. Finally, the precipitating fluxes, particularly for thermal O^+, panel (b), show stochastic precipitation in a stippled pattern on the leading (downstream) hemisphere in the equatorial region (i.e., between ±30° latitude and approximately 45° to 180° W longitude). This precipitation pattern corresponds to thermal Jovian ions that become entrained in Ganymede's reconnection region downstream from the satellite, undergo nonadiabatic motion (i.e., similar to ion motion in the Earth's plasma sheet/tail reconnection region, e.g., Chen & Palmadesso, 1986, or to ion motion in Mercury's magnetotail, e.g., Delcourt & Seki, 2006), become entrained in the quasi-trapped ionic radiation belts (Williams, 2004), and eventually strike the surface of Ganymede. Similar to the precipitation of thermal species in the polar regions, the stochastic nature of the precipitation on the leading hemisphere is presumably representative of continuous precipitation across this entire region of Ganymede by thermal Jovian plasma ions. Finally, we note that overall, precipitation

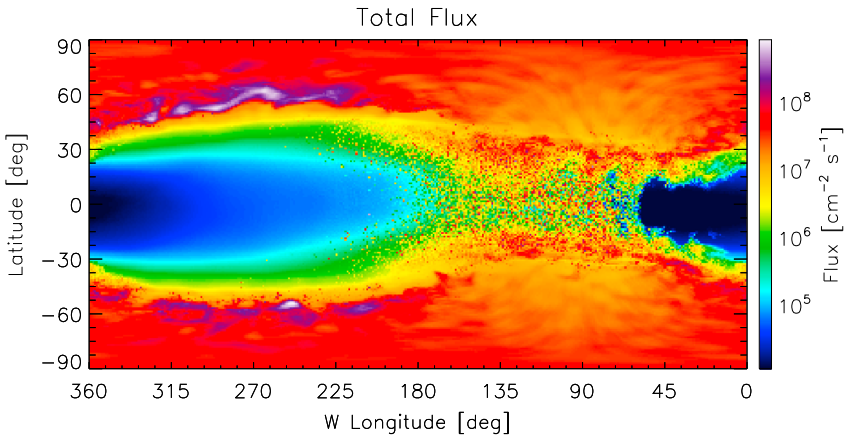

Figure 10. The total ion precipitation flux to the surface of Ganymede, summed over all ion species and energies.

of thermal O^+ ions generally outweighs the precipitation of thermal H^+ ions, mainly reflecting the dominance of O^+ ions in the upstream, Jovian plasma while in the plasma sheet (Kivelson et al., 2004).

Panels 9c–9e show the energetic H^+, O^{++}, and S^{+++} precipitation to the surface of Ganymede, respectively, in the same format as panels (a) and (b). To first order, all three energetic ion species show a large-scale dichotomy in surface fluxes between the polar and equatorial regions of Ganymede, with shielding of precipitating energetic ion fluxes in the equatorial regions by several orders-of-magnitude relative to the polar caps. Furthermore, all three energetic ion species show longitudinal variations in the width of the equatorial shielded region, with the widest latitudinal shielding occurring on the trailing hemisphere (near 270° W longitude) and the narrowest shielding on the leading hemisphere (near 90° W longitude). In the equatorial region of Ganymede, we note that the model does not indicate a perfect shielding from energetic ion species. Both energetic O^{++} and S^{+++} can penetrate Ganymede's magnetosphere down to the surface within the equatorial, closed field line region (i.e., at latitudes less than ±30°). Additionally, the flux of energetic O^{++} and S^{+++} to Ganymede's equatorial region shows a local maximum at longitudes between 135° to 180° , that is, on the slightly Jupiter-averted, leading hemisphere. In particular, one can also see a pair of narrow bands of precipitation in all three energetic species at latitudes of roughly ±30° extending approximately from 0° to 180° W longitude. Both of these features, namely, the broad equatorial precipitation of energetic ions and the formation of narrow bands of precipitation, are consequences of plasma acceleration in Ganymede's magnetotail and the presence of quasi-trapped ion populations in Ganymede's closed field line region (i.e., see discussion of Figure 7 and Galileo EPD observations of trapped ion populations in Williams, 2001). The narrow bands of precipitation correspond to the magnetic footpoints of the open-closed field line boundaries, where particles with field-aligned pitch angles can overcome the magnetic mirror force and precipitate to the surface of Ganymede. The more general precipitation of energetic ions within the equatorial region is more so due to finite-gyroradius effects, whereby trapped energetic ions that have relatively large gyroradii can strike the surface of Ganymede even while being notionally trapped on a Ganymede field line. This also explains the apparent shift of the maximum equatorial precipitation away from the center of the leading hemisphere at 90° towards the anti-Jovian hemisphere, as quasi-trapped ions undergo clockwise drift motion (when viewed from above looking down onto Ganymede's equatorial plane) in addition to bounce motion (see also the 60-keV H^+ trajectory in Figure 6k). The equatorial precipitation of quasi-trapped energetic ions is also a function of ion mass, with heavier S^{+++} yielding more precipitation than O^{++} and O^{++} yielding more equatorial precipitation than H^+. Again, finite gyroradius effects are at play here, whereby the larger ion gyroradii are more likely to strike the surface of Ganymede as they drift around the moon. Figure 10 shows the total ion flux summed over incident energy and species as a function of latitude and longitude on Ganymede's surface. Thermal O^+ is the dominant control for the pattern of flux to Ganymede's surface, with smaller, additional contributions from thermal H^+ and the energetic species.

Figure 11 shows the precipitating ion flux energy spectrum to the surface of Ganymede broken down by region, including the poles, trailing hemisphere, and leading hemisphere, incident ion species, and incident ion energy (at impact). We have defined the polar region as latitudes (either north or south) greater than 60° , while the trailing and leading hemisphere are regions of latitude less than 60° and W longitudes of 180° – 360°

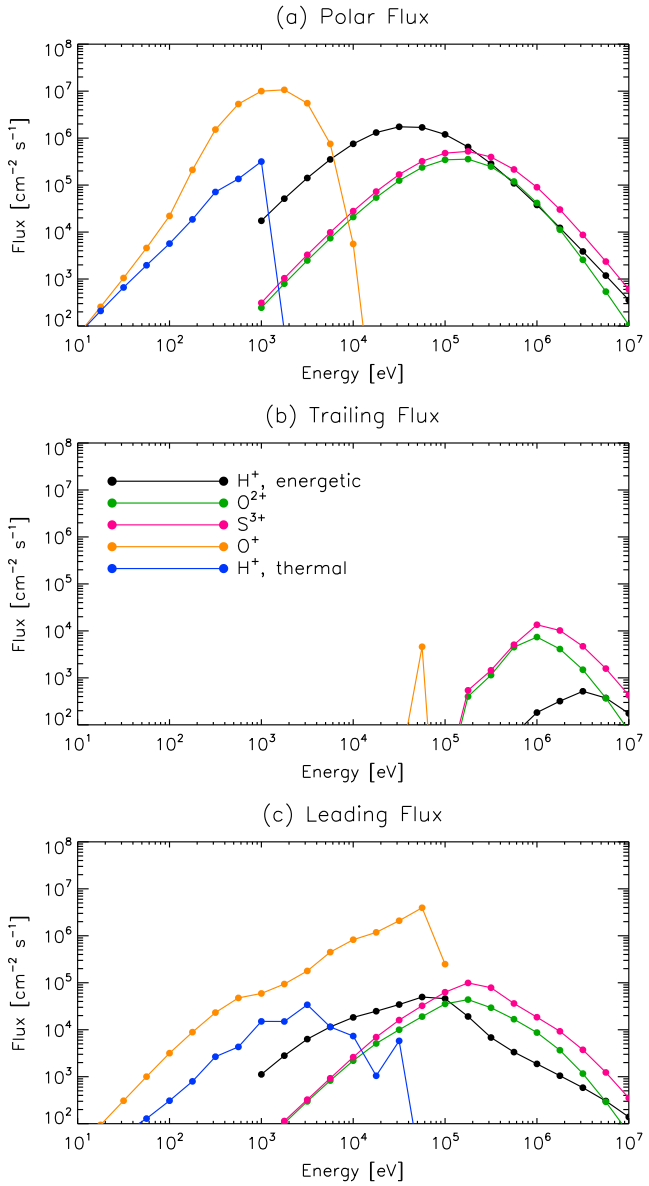

Figure 11. The energy distributions of precipitating ions to Ganymede's surface separated by species, upstream distribution, and surface region of Ganymede.

and 0°–180°, respectively. The flux to the polar region, shown in Figure 11a, contains contributions from both the thermal and energetic ion populations. Thermal H^+ (blue) and O^+ (orange) fluxes peak near 1 keV with a rapid decline in flux for energies greater than 2 and 10 keV for H^+ and O^+, respectively. The energetic ion fluxes peak near 50 keV for H^+ and 200 keV for energetic O^{++} and S^{+++}, as expected from the upstream distributions reported by Mauk et al. (2004) and the open field lines in Ganymede's polar region. Figure 11b shows the flux as a function of energy and species to the trailing hemisphere. Only a small amount of thermal O^+ flux is incident on this hemisphere of Ganymede, as seen in Figures 9a and 9b. Energetic ions, however, can access the trailing hemisphere at relatively lower fluxes ($<\sim 10^4$ cm$^{-2}\cdot$s^{-1} per energy bin) for energies greater than 100 keV for O^{++} and S^{+++} and greater than 1 MeV for energetic H^+. Finally, Figure 11c shows the flux as a function of energy and species to the leading hemisphere. Both thermal and energetic species precipitate to the surface of Ganymede on the leading hemisphere at lower fluxes than in the polar caps, but notably, thermal H^+ and O^+ ions have been accelerated by nearly an order of magnitude in energy. Maximum surface precipitation energies for thermal H^+ and O^+ reach 50 and 100 keV, respectively, indicating that significant energization of these species has occurred as they have interacted with fields near Ganymede, especially within the reconnection region of Ganymede's magnetotail.

Table 1 shows the average ion number fluxes for Ganymede's polar, trailing, and leading regions as a function of ion species. In the polar regions, the dominant ion precipitation is from energetic H^+ and thermal O^+ at fluxes of 8.4×10^6 and 34×10^6 cm$^{-2}\cdot$s^{-1}, respectively, accounting for 90% of the total flux to the polar regions. The total average ion flux in the polar regions of Ganymede is $\approx50\times10^6$ cm$^{-2}\cdot$s^{-1}. In the leading hemisphere, ion fluxes are dominated by thermal O^+ ions at fluxes of 9.2×10^6 cm$^{-2}\cdot$s^{-1} followed by lesser but nearly equal contributions from the three energetic ion species. The total average ion flux to the leading hemisphere of Ganymede is approximately a factor of 5 lower than that in the polar regions. Finally, in the trailing hemisphere, energetic O^{++} and S^{+++} ions deliver most of the flux with only a minor contribution from energetic H^+. The thermal population of ions provides essentially no flux to the trailing hemisphere. Overall, the total average flux in the trailing hemisphere is more than 2 orders-of-magnitude less than in the leading hemisphere or polar regions of Ganymede. While these values fit our first-order expectation of increased fluxes to Ganymede's poles relative to the equatorial region (e.g., Cooper et al., 2001; Khurana et al., 2007), what is perhaps most surprising is the appreciable ion flux to Ganymede's leading hemisphere.

Table 1
Ion Fluxes to the Surface of Ganymede Separated by Incident Species and Region

Species	Polar flux [10^6 cm$^{-2}\cdot$s^{-1}]	Leading flux [10^6 cm$^{-2}\cdot$s^{-1}]	Trailing flux [10^6 cm$^{-2}\cdot$s^{-1}]
H^+, thermal	0.55	0.098	0.00
O^+, thermal	34.0	9.20	0.004
H^+, energetic	8.4	0.23	0.0016
O^{++}, energetic	1.6	0.18	0.019
S^{+++}, energetic	2.4	0.37	0.037
Total	47	10.1	0.058

6. Neutral Sputtering and Exospheric Generation

Remote detections of Ganymede's neutral exosphere include Galileo observations of solar Lyman-α reflected by neutral H atoms (Barth et al., 1997), Hubble Space Telescope UV auroral emissions from atomic O (Hall et al., 1998; Feldman et al., 2000; McGrath et al., 2013), and Hubble Space Telescope observations of atomic H (Feldman et al., 2000). These observations imply significant neutral H_2 and O_2 populations in additional to smaller contributions from atomic H and O. The two main processes responsible for neutral exospheric generation at Ganymede are thermal sublimation and charged particle sputtering (i.e., Johnson, 1990; Johnson et al., 2004). At Jupiter's heliocentric distance, direct sublimation is only effective near Ganymede's subsolar point where temperatures reach approximately 150 K (Orton et al., 1996; Spencer, 1987), producing a local, semicollisional water (and water group) neutral exosphere. In contrast, charged particle sputtering of the surface is governed by a combination of the upstream Jovian plasma and energetic particle environment and the electromagnetic structure of Ganymede's magnetosphere. Thus, previous work has generally accepted that Ganymede's equatorial region should be protected from direct particle impact leaving only the polar regions exposed to sputtering.

Assuming this polar/equatorial dichotomy, Marconi (2007) presented an early, two-dimensional model of Ganymede's neutral exosphere that distinguished between a sputtered exosphere in the polar regions and a semicollisional, sublimated H_2O exosphere centered on the subsolar point. H_2 and O_2 are the dominant neutrals ejected from Ganymede's surface due to sputtering and radiolysis and form the dominant constituents of the polar exosphere. Later works by Turc et al. (2014), Plainaki et al. (2015), and Leblanc et al. (2017) have extended the work of Marconi (2007) to three dimensions and generally found similar results. Despite these investigations into Ganymede's neutral exosphere, we lack a full understanding of the absolute flux, spatial distribution, and inherent variability of neutrals sputtered from Ganymede's surface by incident Jovian ions. Cooper et al. (2001) performed ion tracing through Ganymede's magnetosphere with only superimposed magnetic fields and no electric fields, and Plainaki et al. (2015) calculated surface precipitation fluxes from an MHD/particle-tracing model for Jovian H^+, O^+, and S^+ ion species at a selection of discrete energies. Here we use the energetic ion precipitation maps for Ganymede's surface presented here in Figure 9 to construct a more complete picture of the neutral sputtering rates and spatial distributions that feed into Ganymede's neutral exosphere.

Figure 12a shows the neutral sputtering yield for icy surfaces as a function of incident ion energy for the three ion species used here, H^+, O^{n+}, and S^{n+} at surface temperatures <100 K (Johnson et al., 2004). The functional forms of the yields, Y_i, where i denotes incident ion species, are given by

$$\frac{1}{Y_i} = \frac{1}{Y_{Li}} + \frac{1}{Y_{Hi}}, \tag{1}$$

where

$$Y_{Hi} = 11.2 Z_i^{2.8} \left(v / Z_i^{1/3} \right)^{-2.24}, \tag{2}$$

$$Y_{Li} = 4.2 Z_i^{2.8} \left(v / Z_i^{1/3} \right)^{2.16}, \tag{3}$$

Z_i is the nuclear charge of the incident ion, and v is the velocity of the incident ion in atomic units (1 atomic unit = 2.18×10^8 cm/s; Johnson et al., 2004). Thus, as shown in Figure 12a, the peak sputtering yields for H^+, O^{n+}, and S^{n+} occur at approximately 40 keV, 2.5 MeV, and 8 MeV, respectively. We also note that sputtering yields from icy surfaces have been shown to be temperature dependent, with constant yields at temperatures less than 100 K followed by rapid increases for surface temperatures >100 K (e.g., Baragiola et al., 2003; Johnson et al., 2004; Shi et al., 1995). For example, sputtering yields for 30-keV O^+ onto ice increase fivefold from $T < 90$ K to $T = 150$ K (Shi et al., 1995), which is the relevant range of surface temperatures of Ganymede (Orton et al., 1996). For the analysis here we do not include temperature dependence of the icy surface (e.g., such as that done by Plainaki et al., 2013, for Europa), leaving more detailed work (which would include, e.g., variations in the relative orientation of the subsolar point with the GPhiO coordinate system) to future work.

To compute the neutral sputtered flux from the surface of Ganymede as a function of region, incident ion species, and incident ion energy, we convolve the incident ion fluxes presented in Figure 11 with the appropriate neutral sputtering yields from Figure 12a. Panels 12b–12d show the sputtered neutral flux per energy

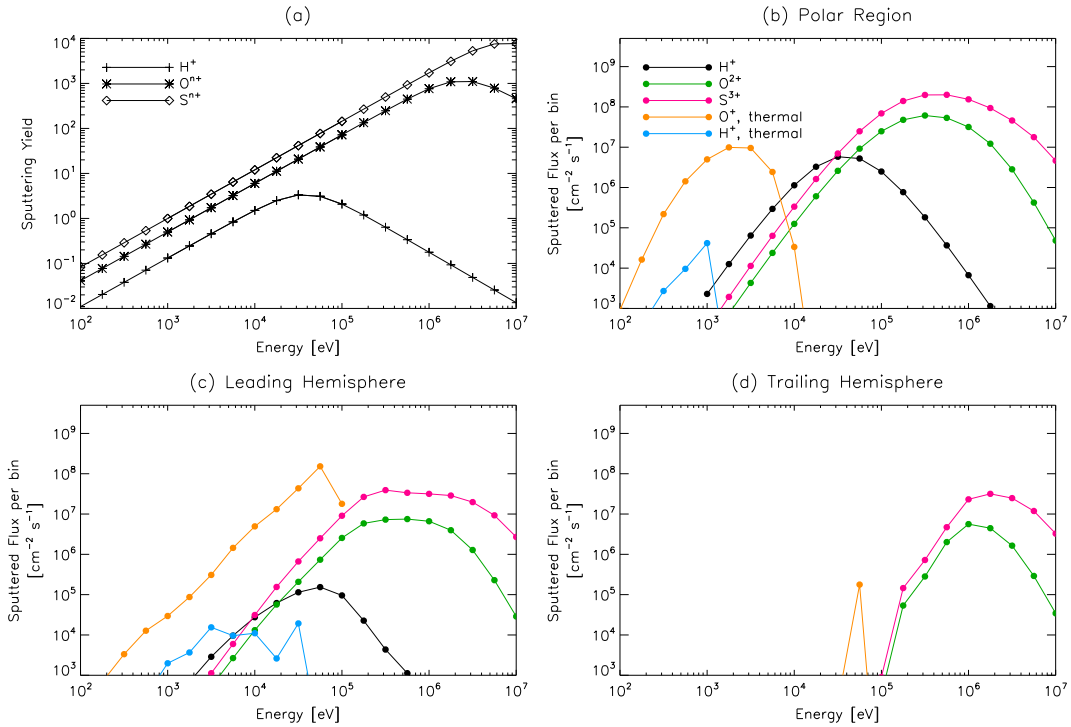

Figure 12. (a) The neutral sputtering yields as a function of ion energy and species from 10^2 to 10^7 eV for icy surfaces at temperatures <100 K (Johnson et al., 2004). (b–d) The neutral sputtered flux per energy bin as a function of ion species and energy for different regions on Ganymede.

bin as a function of incident ion energy and species for the polar region, leading hemisphere, and trailing hemisphere, respectively. In the polar region, sputtered contributions are dominated by the energetic S^{+++} and O^{++} with moderate contributions from energetic H^+ and thermal O^+, and only a minor contribution from thermal H^+. The emphasis of the heavier incident ions with respect to the sputtering is expected given the large increase in sputtering yield as a function of ion mass, that is, Figure 12a (see also, e.g., Johnson et al., 2004). The leading hemisphere, Figure 12c, is dominated by energetic S^{+++} and O^{++} but also has a stronger contribution from thermal O^+ ions that have been accelerated before impact onto Ganymede's surface. Thermal and energetic H^+ ions provide only minor contributions to the sputtered neutral flux here. Finally, in the trailing hemisphere, the shielding of both thermal species (H^+ and O^+) and energetic H^+ leaves only energetic S^{+++} and O^{++} at energies greater than 10^5 eV as a source of sputtered neutrals, albeit at fluxes equivalent to those in the leading hemisphere for similar energies. Overall, the average sputtered flux for the polar, leading, and trailing regions, found by summing over both species and energy, is 1.3×10^9, 4.8×10^8, and 1.2×10^8 cm$^{-2} \cdot$ s^{-1}, respectively.

Thus, we find somewhat surprisingly that neutral sputtering is only reduced by factors of 2.5 and 10 in the leading and trailing hemispheres, respectively, rather than a complete reduction of sputtering within Ganymede's equatorial region. We show the net sputtered flux, summed over incident ion energy and species, as a function of latitude and W longitude on Ganymede's surface in Figure 13. The sputtered flux distribution shares many of the same characteristics with the total incident ion flux shown in Figure 10, including peak sputtering in the polar cap regions, suppressed yet still significant sputtering in the equatorial region, narrow bands of enhanced sputtering on the trailing (upstream) hemisphere due to the heavy precipitation of thermal ions along the open-closed field line boundary, and a region of enhanced sputtering on the leading hemisphere within ±30° due to the precipitation of quasi-trapped ions (especially thermal O^+) along Ganymede's closed field line region. The relative strengths of these various features are somewhat different than those shown in Figure 10, due to the fact that the neutral sputtering yields are strongly correlated with impacting ion mass and thus features due to S^{n+} and O^{n+} ion precipitation are more heavily weighted than those from H^+.

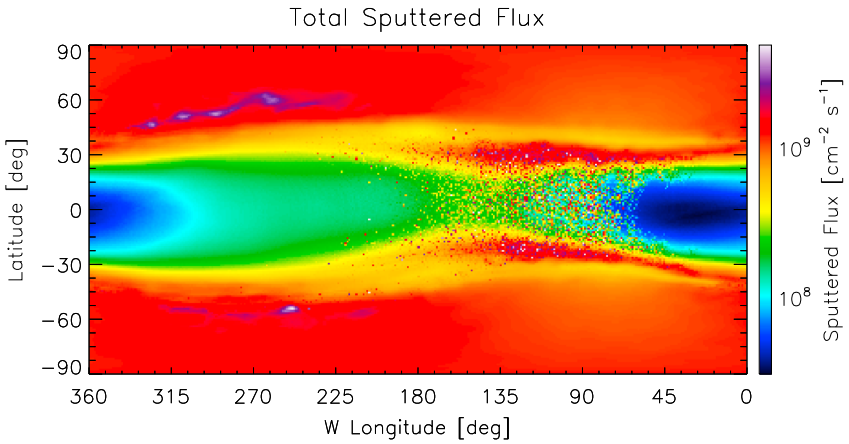

Figure 13. The spatial distribution of the total neutral sputtered flux from the surface of Ganymede due to both thermal and energetic Jovian ions.

7. Discussion

Our results here can be compared with previous modeling of energetic ion access to the surface of Ganymede. Cooper et al. (2001) used both an analytic theory (Størmer, 1955) and a backwards Liouville tracing technique similar to that used here to quantify charged particle access to Ganymede's surface. Notably, however, Cooper et al. (2001) did not use a self-consistent plasma model (either MHD or hybrid, for example) for the background electric and magnetic fields, but rather a superposition of Ganymede's internal field and the ambient Jovian field. Despite this limitation, Cooper et al. (2001) found in Ganymede's equatorial region that (1) protons with energy below 20 keV show a longitudinal asymmetry at Ganymede's magnetic equator with more particle access to the trailing hemisphere than the leading hemisphere, (2) protons with intermediate energies (i.e., 20 keV $< E <$ 5 MeV) have no access to Ganymede's equatorial region but can access the surface for magnetic latitudes greater than 30°, and (3) protons with energies greater than 5 MeV have near uniform access to the equatorial region, regardless of longitude. Cooper et al. (2001) duly noted that a more accurate characterization of surface precipitation would require a more self-consistent model for both the compression of Ganymede's field lines and the presence of various electric fields. Thus, having employed such a method here with the hybrid modeling results of Fatemi et al. (2016), our results appear somewhat different from the conclusions drawn in Cooper et al. (2001). In Ganymede's equatorial region, we see that only energetic O^{++} and S^{+++} are able to precipitate to the trailing hemisphere via bounce-drift motion along quasi-trapped orbits. This mechanism of particle precipitation yields a longitudinal asymmetry in the equatorial surface flux, with most flux on the Jupiter-averted hemisphere of Ganymede. Energetic protons, meanwhile, are unable to reach Ganymede's surface in the equatorial region (i.e., see Figure 9c). Furthermore, our simulations provide no low-energy ($E <$ 20 keV) ion flux to Ganymede's trailing hemisphere but, in contrast, do show low-energy ion access to Ganymede's leading hemisphere due to entrainment and precipitation from Ganymede's magnetotail and current sheet.

Allioux et al. (2013) modeled the flux of energetic ions in near-Ganymede space in an effort to predict the radiation environment for future Ganymede orbital missions. Similar to Cooper et al. (2001), Allioux et al. (2013) used a superposition of Ganymede and Jovian magnetic fields as background fields rather than the results of a self-consistent plasma model. Their results for 25 keV, 300 keV, and 6 MeV H^+ and O^{++} densities in near-Ganymede space display local depletions mainly centered over the polar regions of Ganymede, within the closed field line region in Ganymede's equatorial region, and near the "cusp" regions where the total fields reach a minimum in the simple superposition model of magnetic fields. The results of Allioux et al. (2013) do show a general decrease in ion density dropouts as the ion energy increases. Qualitatively, some of the features identified in Allioux et al. (2013) are similar to those found here for particle tracing a self-consistent hybrid plasma fields. This includes the decrease in flux over the poles of Ganymede and the (mostly) shielded region in Ganymede's equatorial region (i.e., compare Figures 7 and 8 here to Figure 2 of Allioux et al., 2013). In contrast, however, inclusion of the self-consistent electric and magnetic fields alters the near-Ganymede energetic particle environment in critical ways. This includes, for example, the asymmetric distortion of features

in Ganymede's magnetosphere due to the ambient Jovian pressure, the development of quasi-trapped ion distributions in Ganymede's equatorial region via Ganymede's magnetotail, and the acceleration of thermal Jovian ions to energies up to 10^5 eV and their subsequent precipitation to the surface. These effects rely on capturing accurate, self-consistent plasma effects within Ganymede's magnetosphere.

Our results hew most closely perhaps to those of Plainaki et al. (2015), who simulated the flux of Jovian ions near and onto the surface of Ganymede using electric and magnetic fields from the MHD models of Jia et al. (2008) and Jia et al. (2009). The flux of Jovian O^+ ions in near-Ganymede space at three different energies (shown in Figure 1 of Plainaki et al., 2015) shares many of the same features as our particle tracing results shown here in Figures 7 and 8, notwithstanding the different charge state we assume for oxygen (O^{++}) as opposed to Plainaki et al. (O^+). Both simulations show a shielded region close to Ganymede ($r < 1.5\ R_G$) asymmetrically displaced towards the sub-Jovian, trailing hemisphere, enhancements of lower-energy ion flux along the trailing-side boundaries of Ganymede's Alfvén wings, and enhancements in the flux on the anti-Jovian, leading hemisphere. Finally, higher energy ions in both simulations are less affected by the fields of Ganymede's magnetosphere and thus more isotropic in near-Ganymede space. Finally, while Figure 2 of Plainaki et al. (2015) only shows the precipitating flux of Jovian O^+ ions to the surface of Ganymede, these results (at least for their assumption of mirroring ions) agrees moderately well with our calculations of precipitating oxygen flux. This includes strong fluxes to the polar regions, a moderate amount of precipitation in the equatorial, leading hemisphere, and strongly suppressed ion fluxes to Ganymede's trailing, equatorial hemisphere. We do comment here that the simulation method used in our analysis (i.e., the backwards Liouville tracing) does not utilize a mirroring assumption for the ions as does Plainaki et al. (2015). Jovian ions of all relevant species at energies less than tens of MeV cannot complete a half bounce period (i.e., from the equatorial plane to Jupiter's polar region and back to the equatorial plane) within the amount of time that the Jovian plasma notionally corotates past Ganymede (electrons, on the other hand, can bounce fast enough, e.g., Williams & Mauk, 1997). Thus, while the tracing results of Plainaki et al. (2015) do produce precipitating polar cap ion fluxes at Ganymede under the assumption of mirroring ions, it is not clear that this mirroring assumption is the correct fundamentally underlying mechanism.

The neutral sputtered fluxes calculated in section 6 can also be used to estimate the net mass loss of material from the surface of Ganymede. Integrating the sputtered fluxes shown in Figure 13 over surface area, we calculate the net sputtering rate to be $\approx 7 \times 10^{26}$ s^{-1}, approximately a factor of 2 higher than that estimated in Ip et al. (1997) and a factor of 10 higher than that calculated in Plainaki et al. (2015). While the factor of two difference between our results and Ip et al. (1997) can easily be attributed to estimation, the difference of an order of magnitude between our results and Plainaki et al. (2015) is most likely due to the fact that Plainaki et al. (2015) limited their impacting magnetospheric ion energy to a maximum of 100 keV. Inspection of the sputtered fluxes versus impacting ion energy shown here in Figure 12 shows that ions with energies greater than 100 keV play a significant role in neutral sputtering. This is especially true for O^{++} and S^{+++}, whose production of sputtered neutrals peaks between 500 keV and 2 MeV, depending on the region of Ganymede. The net mass loss rate from Ganymede due to sputtering can also be estimated. Assuming a mean molecular mass of 18 amu (H_2O) and using a direct escape fraction of 33% for sputtered water molecules from an icy body the size of Ganymede (taken from Killen et al., 2017), the sputtered mass loss from Ganymede is on the order of 22 kg/s. This is a relatively small value compared to that injected by Io, $\sim 10^3$ kg/s (e.g., Dessler, 1980; Thomas et al., 2004) but is only approximately half of that estimated for Europa, ~50 kg/s (e.g., Saur et al., 1998; Schreier et al., 1993), (neglecting any possible contribution from plumes).

Finally, the evolution of Ganymede's surface by charged-particle irradiation can be interpreted in light of the ion precipitation results derived here. As first pointed out by Smith et al. (1979) based on Voyager observations and later confirmed by Galileo imaging (Johnson, 1997; Khurana et al., 2007), Ganymede possesses a distinct surficial albedo dichotomy between the bright polar caps and the relatively dark equatorial region. Furthermore, Ganymede's equatorial region possesses itself a leading/trailing asymmetry, with a relatively bright leading hemisphere compared to a darker trailing hemisphere (Clark et al., 1986). Khurana et al. (2007) noted that the brightness boundary on Ganymede's surface corresponds closely with the open/closed field line boundary of Ganymede's magnetosphere and thus ascribed the polar cap formation to precipitation of energetic Jovian ions, which serves to sputter and redistribute water frost onto optically thick material, thereby brightening the surface albedo. Khurana et al. (2007) also postulated that the equatorial leading/trailing asymmetry was due to the preferential flux of ions onto Ganymede's leading hemisphere

via ion capture in Ganymede's magnetotail reconnection region. Our results here confirm the conclusions of Khurana et al. (2007) and our earlier work in Fatemi et al. (2016) with respect to both points. In particular, while the preferential access of Jovian ions to Ganymede's polar caps is a relatively straightforward conclusion from the magnetic topology at Ganymede, the precipitation of energetic ions on Ganymede's leading hemisphere has been further elucidated from the particle tracing results shown here. Our results demonstrate that the highly kinetic, nonadiabatic motion of ions within Ganymede's magnetotail and along quasi-trapped equatorial orbits must be fully resolved in order to accurately map precipitation to the surface.

8. Conclusion

We have used the combination of electric and magnetic fields derived from hybrid simulations of Ganymede's magnetosphere (Fatemi et al., 2016) and a backwards Liouville tracing technique to quantify the dynamics of thermal and energetic ions near Ganymede. Having specified the upstream plasma conditions for both the thermal (Kivelson et al., 2004) and energetic (Mauk et al., 2004) components of Jupiter's plasma environment, we have computed the flux of Jovian ions in near-Ganymede space and the precipitating flux of Jovian ions to the surface of Ganymede. Within near-Ganymede space, our models predict several features of note, including a shielded equatorial region on Ganymede's trailing hemisphere and the presence of quasi-trapped ionic radiation belts mainly on Ganymede's Jupiter-averted hemisphere. In particular, the presence of quasi-trapped distributions supports previous analyses of Galileo EPD measurements taken during various Ganymede flybys (Williams, 2001, 2004). Our model predicts precipitation of Jovian thermal and energetic ions mainly to the polar regions of Ganymede but also, we find nonnegligible precipitation in the equatorial region. This latter source of precipitation is due to the intersection of quasi-trapped ion orbits in Ganymede's equatorial region with the surface. We have also computed the neutral sputtering rates due to ion precipitation to the surface of Ganymede finding again dominant production of sputtered neutrals in the polar regions and reduced, although nonzero production of sputtered neutrals in Ganymede's equatorial region. Taken as a whole, these results confirm the utility of the backwards Liouville tracing technique and the application of a kinetic model (at least with respect to the ions) in understanding the fundamental nature of plasma interactions in Ganymede's magnetosphere and the subsequent implications of this kinetic ion behavior for the evolution of Ganymede's surface and exosphere.

Future work based on these results will model the formation of the Ganymedean exosphere and in combination with the hybrid model of Fatemi et al. (2016) will examine the ionization and outflow of ionospheric species from Ganymede. Paty et al. (2008) and Jia et al. (2008) have previously modeled the outflow of Ganymedean ions using a multifluid model with general agreement with Galileo PLS observations. The hybrid model, by treating ions as particles as opposed to a fluid, offers the ability to quantify the kinetic nature of cold ion outflow at Ganymede. Pickup ion dynamics is an inherently kinetic process and newly born ions from Ganymede's exosphere may be expected to undergo complex, nonadiabatic motion due reconnection and/or small-scale features (i.e., those less than a gyroradius) in Ganymede's magnetosphere. Thus, the circulation, recycling, and potential escape of Ganymedean ions is a subject of study well-suited for a hybrid model.

Many of the simulation results presented here can be critically tested and compared with future results both NASA's Europa Clipper mission and ESA's Jupiter Icy Moons (JUICE) mission (Grasset et al., 2013). The Europa Clipper mission, while focused on Europa, may potentially make measurements of Ganymede's magnetosphere during possible flybys. Meanwhile, JUICE will notionally launch in 2022 followed by a 7 year cruise to Jupiter. After approximately two additional years of circum-Jovian observations, JUICE will enter into orbit around Ganymede. The orbital tour of Ganymede by JUICE is planned to consist of a high altitude (5,000 km), medium altitude (500 km), and low altitude (200 km) series of orbits, interspersed with periodic elliptical orbital transfers. JUICE will be equipped with (among other instruments) a magnetometer and particle spectrometers covering a wide range in energy. Thus, a complete mapping of Ganymede's magnetosphere, it's interaction with the Jovian magnetosphere, and the resulting precipitation of Jovian ions to the surface of Ganymede will be conducted by JUICE. Models of Ganymede's magnetosphere (e.g., Fatemi et al., 2016) and complementary models of energetic ion dynamics in Ganymede's magnetosphere such as those presented here will be an invaluable tool for understanding and interpreting the anticipated observations of both these missions.

Acknowledgments
The authors gratefully acknowledge support from NASA's Solar System Workings Program grant NNX16AR99G. The authors also thank two anonymous reviewers for constructive reviews. The model results are publicly available at https://doi.org/10.6078/D1BT11.

References

Allioux, R., Louarn, P., & André, N. (2013). Model of energetic populations at Ganymede, implications for an orbiter. *Advances in Space Research*, *51*, 1204–1212.

Bagenal, F., Wilson, R. J., Siler, S., Paterson, W. R., & Kurth, W. S. (2016). Survey of Galileo plasma observations in Jupiter's plasma sheet. *Journal of Geophysical Research: Planets*, *121*, 871–894. https://doi.org/10.1002/2016JE005009

Bahr, D. A., Famá, M., Vidal, R. A., & Baragiola, R. A. (2001). Radiolysis of water ice in the outer solar system: Sputtering and trapping of radiation products. *Journal of Geophysical Research*, *106*(E12), 33,285–33,290.

Baragiola, R. A., Vidal, R. A., Svendsen, W., Schou, J., Shi, M., Bahr, D. A., & Atteberry, C. L. (2003). Sputtering of water ice. *Nuclear Instruments and Methods in Physics Research Section B*, *209*, 294–303.

Barth, C. A., Hord, C. W., Stewart, A. I. F., Pryor, W. R., Simmons, K. E., McClintock, W. E., et al. (1997). Galileo ultraviolet spectrometer observations of atomic hydrogen in the atmosphere of Ganymede. *Geophysical Research Letters*, *24*(17), 2147–2150.

Chen, J., & Palmadesso, P. J. (1986). Chaos and nonlinear dynamics of single-particle orbits in a magnetotaillike magnetic field. *Journal of Geophysical Research*, *91*(A2), 1499–1508.

Clark, R. N., Fanale, F. P., & Gaffey, M. J. (1986). Surface composition of natural satellites. In J. A. Burns & M. S. Matthews (Eds.), *IAU Colloq. 77: Some background about satellites* (pp. 437–491). Tuscon: University of Arizona Press.

Collier, M. R., & Hamilton, D. C. (1995). The relationship between kappa and temperature in energetic ion spectra at Jupiter. *Geophysical Research Letters*, *22*(3), 303–306.

Cooper, J. F., Johnson, R. E., Mauk, B. H., Garrett, H. B., & Gehrels, N. (2001). Energetic ion and electron irradiation of the icy Galilean satellites. *Icarus*, *149*, 133–159.

Delcourt, D. C., & Seki, K. (2006). On the dynamics of charged particles in the magnetosphere of Mercury. In *Advances in Geosciences* (Vol. 3, p. 17). Singapore: Published by World Scientific Co., Pte. Ltd.

Dessler, A. J. (1980). Mass-injection rate from Io into the Io plasma torus. *Icarus*, *44*(2), 291–295.

Dorelli, J. C., Glocer, A., Collinson, G., & Tóth, G. (2015). The role of the Hall effect in the global structure and dynamics of planetary magnetospheres: Ganymede as a case study. *Journal of Geophysical Research: Space Physics*, *120*, 5377–5392. https://doi.org/10.1002/2014JA020951

Duling, S., Saur, J., & Wicht, J. (2014). Consistent boundary conditions at nonconducting surfaces of planetary bodies: Applications in a new Ganymede MHD model. *Journal of Geophysical Research: Space Physics*, *119*, 4412–4440. https://doi.org/10.1002/2013JA019554

Dungey, J. W. (1961). Interplanetary magnetic field and the auroral zones. *Physical Review Letters*, *6*, 47–48.

Eviatar, A., Strobel, D. F., Wolven, B. C., Feldman, P. D., McGrath, M. A., & Williams, D. J. (2001). Excitation of the Ganymede ultraviolet aurora. *The Astrophysical Journal*, *555*, 1013–1019.

Eviatar, A., Vasyliunas, V. M., & Gurnett, D. A. (2001). The ionosphere of Ganymede. *Planetary and Space Science*, *49*, 327–336.

Eviatar, A., Williams, D. J., Paranicas, C., McEntire, R. W., Mauk, B. H., & Kivelson, M. G. (2000). Trapped energetic electrons in the magnetosphere of Ganymede. *Journal of Geophysical Research*, *105*(A3), 5547–5553.

Famá, M., Loeffler, M. J., Raut, U., & Baragiola, R. A. (2010). Radiation-induced amorphization of crystalline ice. *Icarus*, *207*, 314–319.

Fatemi, S., Holmström, M., & Futaana, Y. (2012). The effects of lunar surface plasma absorption and solar wind temperature anisotropies on the solar wind proton velocity space distributions in the low-altitude lunar plasma wake. *Journal of Geophysical Research*, *117*, A10105. https://doi.org/10.1029/2011JA017353

Fatemi, S., Poppe, A. R., Khurana, K. K., Holmström, M., & Delory, G. T. (2016). On the formation of Ganymede's surface brightness asymmetries: Kinetic simulations of Ganymede's magnetosphere. *Geophysical Research Letters*, *43*, 4745–4754. https://doi.org/10.1002/2016GL068363

Feldman, P. D., McGrath, M. A., Strobel, D. F., Moos, H. W., Retherford, K. D., & Wolven, B. C. (2000). HST/STIS ultraviolet imaging of polar aurora on Ganymede. *The Astrophysical Journal*, *535*, 1085–1090.

Frank, L. A., Ackerson, K. L., Lee, J. A., English, M. R., & Pickett, G. L. (1992). The plasma instrumentation for the Galileo mission. *Space Science Reviews*, *60*, 283–307.

Frank, L. A., Paterson, W. R., Ackerson, K. L., & Bolton, S. J. (1997). Outflow of hydrogen ions from Ganymede. *Geophysical Research Letters*, *24*(17), 2151–2154.

Gomis, O., Satorre, M. A., Strazzulla, G., & Leto, G. (2004). Hydrogen peroxide formation by ion implantation in water icy and its relevance to the Galilean satellites. *Planetary and Space Science*, *52*, 371–378.

Grasset, O., Dougherty, M. K., Coustenis, A., Bunce, E. J., Erd, C., Titov, D., et al. (2013). JUpiter ICy moons Explorer (JUICE): An ESA mission to orbit Ganymede and to characterize the Jupiter system. *Planetary and Space Science*, *78*, 1–21.

Gurnett, D. A., Kurth, W. S., Roux, A., Bolton, S. J., & Kennel, C. F. (1996). Evidence for a magnetosphere at Ganymede from plasma-wave observations by the Galileo spacecraft. *Nature*, *384*, 535–537.

Hall, D. T., Feldman, P. D., McGrath, M. A., & Strobel, D. F. (1998). The far-ultraviolet airglow of Europa and Ganymede. *The Astrophysical Journal*, *499*, 475–481.

Hansen, G. B., & McCord, T. B. (2004). Amorphous and crystalline ice on the Galilean satellites: A balance between thermal and radiolytic processes. *Journal of Geophysical Research*, *109*, E01012. https://doi.org/10.1029/2003JE002149

Ip, W.-H., Williams, D. J., McEntire, R. W., & Mauk, B. (1997). Energetic ion sputtering effects at Ganymede. *Geophysical Research Letters*, *24*(21), 2631–2634.

Jia, X., Walker, R. J., Kivelson, M. G., Khurana, K. K., & Linker, J. A. (2008). Three-dimensional MHD simulations of Ganymede's magnetosphere. *Journal of Geophysical Research*, *113*, A06212. https://doi.org/10. 1029/2007JA012748

Jia, X., Walker, R. J., Kivelson, M. G., Khurana, K. K., & Linker, J. A. (2009). Properties of Ganymede's magnetosphere inferred from improved three-dimensional MHD simulations. *Journal of Geophysical Research*, *114*, A09209. https://doi.org/10.1029/2009JA014375

Jia, X., Walker, R. J., Kivelson, M. G., Khurana, K. K., & Linker, J. A. (2010). Dynamics of Ganymede's magnetopause: Intermittent reconnection under steady external conditions. *Journal of Geophysical Research*, *115*, A12202. https://doi.org/10.1029/2010JA015771

Johnson, R. E. (1990). Interactions with surfaces. *Energetic charged-particle interactions with atmospheres and surfaces* (pp. 75–135). Berlin: Springer-Verlag.

Johnson, R. E. (1997). Polar "Caps" on Ganymede and Io revisited. *Icarus*, *128*, 469–471.

Johnson, R. E., Carlson, R. W., Cooper, J. F., Paranicas, C., Moore, M. H., & Wong, M. C. (2004). Radiation effects on the surfaces of the Galilean satellites. In R. E. Johnson, R. W. Carlson, J. F. Cooper, C. Paranicas, M. H. Moore, & M. C. Wong (Eds.), *Jupiter: The planet, satellites, and magnetosphere* (pp. 483–510). Cambridge, UK: Cambridge University Press.

Kane, M., Williams, D. J., Mauk, B. H., McEntire, R. W., & Roelof, E. C. (1999). Galileo energetic particles detector measurements of hot ions in the neutral sheet region of Jupiter's magnetodisk. *Geophysical Research Letters*, *26*, 5–8.

Kasahara, S., Kronberg, E. A., Krupp, N., Kimura, T., Tao, C., Badman, S. V., et al. (2011). Magnetic reconnection in the Jovian tail: X-line evolution and consequent plasma sheet structures. *Journal of Geophysical Research*, *116*, A11219. https://doi.org/10.1029/2011JA016892

Keppler, E., & Krupp, N. (1996). The charge state of helium in the Jovian magnetosphere: A possible method to determine it. *Planetary and Space Science*, *44*(2), 71–75.

Khurana, K. K., Pappalardo, R. T., Murphy, N., & Denk, T. (2007). The origin of Ganymede's polar caps. *Icarus*, *191*, 193–202.

Killen, R. M., Burger, M. H., & Farrell, W. M. (2017). Exospheric escape: A parametrical study. *Advances in Space Research*. https://doi.org/10.1016/j.asr.2017.06.015

Kivelson, M. G., Bagenal, F., Kurth, W. S., Neubauer, F. M., Paranicas, C., & Saur, J. (2004). Magnetospheric interactions with satellites, *Jupiter: The planet, satellites, and magnetosphere* (pp. 513–536). Cambridge, UK: Cambridge University Press.

Kivelson, M. G., Khurana, K. K., Russell, C. T., Walker, R. J., Warnecke, J., Coroniti, F. V., et al. (1996). Discovery of Ganymede's magnetic field by the Galileo spacecraft. *Nature*, *384*, 537–541.

Kivelson, M. G., Khurana, K. K., & Volwerk, M. (2002). The permanent and inductive magnetic moments of Ganymede. *Icarus*, *157*, 507–522.

Kivelson, M. G., Warnecke, J., Bennett, L., Joy, S., Khurana, K. K., Linker, J. A., et al. (1998). Ganymede's magnetosphere: Magnetometer overview. *Journal of Geophysical Research*, *103*(E9), 19,963–19,972.

Kopp, A., & Ip, W.-H. (2002). Resistive MHD simulations of Ganymede's magnetosphere 1. Time variabilities of the magnetic field topology. *Journal of Geophysical Research*, *107*(A12), 1490.

Kronberg, E. A., Woch, J., Krupp, N., & Lagg, A. (2008). Mass release process in the Jovian magnetosphere: Statistics on particle burst parameters. *Journal of Geophysical Research*, *113*, A10202. https://doi.org/10.1029/2008JA013332

Leblanc, F., Oza, A. V., Leclerq, L., Schmidt, C., Cassidy, T., Modolo, R., et al. (2017). On the orbital variability of Ganymede's atmosphere. *Icarus*, *293*, 185–198.

Marconi, M. L. (2007). A kinetic model of Ganymede's atmosphere. *Icarus*, *190*, 155–174.

Martin, R. F. (1986). Chaotic particle dynamics near a two dimensional magnetic neutral point with application to the geomagnetic tail. *Journal of Geophysical Research*, *91*, 11,985–11,992.

Mauk, B. H., Mitchell, D. G., McEntire, R. W., Paranicas, C. P., Roelof, E. C., Williams, D. J., et al. (2004). Energetic ion characteristics and neutral gas interactions in Jupiter's magnetosphere. *Journal of Geophysical Research*, *109*, A09S12. https://doi.org/10.1029/2003JA010270

McGrath, M. A., Jia, X., Retherford, K., Feldman, P. D., Strobel, D. F., & Saur, J. (2013). Aurora on Ganymede. *Journal of Geophysical Research: Space Physics*, *118*, 2043–2054. https://doi.org/10.1002/jgra.50122

Moore, M. H., Hudson, R. L., & Carlson, R. W. (2007). The radiolysis of SO_2 and H_2S in water ice: Implications for the icy Jovian satellites. *Icarus*, *189*, 409–423.

Musacchio, F., Saur, J., Roth, L., Retherford, K. D., McGrath, M. A., Feldman, P. D., & Strobel, D. F. (2017). Morphology of Ganymede's FUV auroral ovals. *Journal of Geophysical Research: Space Physics*, *122*, 2855–2876. https://doi.org/10.1002/2016JA023220

Orton, G. S., Spencer, J. R., Travis, L. D., Martin, T. Z., & Tamppari, L. K. (1996). Galileo photopolarimeter-radiometer observations of Jupiter and the Galilean satellites. *Science*, *274*, 389–391.

Paranicas, C., Paterson, W. R., Cheng, A. F., Mauk, B. H., McEntire, R. W., Frank, L. A., & Williams, D. J. (1999). Energetic particle observations near Ganymede. *Journal of Geophysical Research*, *104*(8), 17,459–17,469.

Paty, C., Paterson, W., & Winglee, R. (2008). Ion energization in Ganymede's magnetosphere: Using multifluid simulations to interpret ion energy spectrograms. *Journal of Geophysical Research*, *113*, A06211. https://doi.org/10.1029/2007JA012848

Paty, C., & Winglee, R. (2004). Multi-fluid simulations of Ganymede's magnetosphere. *Geophysical Research Letters*, *31*, L24806. https://doi.org/10.1029/2004GL021220

Paty, C., & Winglee, R. (2006). The role of ion cyclotron motion at Ganymede: Magnetic field morphology and magnetospheric dynamics. *Geophysical Research Letters*, *33*, L10106. https://doi.org/10.1029/2005GL025273

Payan, A. P., Paty, C. S., & Retherford, K. D. (2015). Uncovering local magnetospheric processes governing the morphology and variability of Ganymede's aurora using three-dimensional multifluid simulations of Ganymede's magnetosphere. *Journal of Geophysical Research: Space Physics*, *120*, 401–413. https://doi.org/10.1002/2014JA020301

Plainaki, C., Milillo, A., Massetti, S., Mura, A., Jia, X., Orsini, S., et al. (2015). The H_2O and O_2 exospheres of Ganymede: The result of a complex interaction between the Jovian magnetospheric ions and the icy moon. *Icarus*, *245*, 306–319.

Plainaki, C., Milillo, A., Mura, A., Saur, J., Orsini, S., & Massetti, S. (2013). Exospheric O_2 densities at Europa during different orbital phases. *Planetary and Space Science*, *88*, 42–52.

Poppe, A. R., Halekas, J. S., Lue, C., & Fatemi, S. (2017). ARTEMIS observations of the solar wind proton scattering function from lunar crustal magnetic anomalies. *Journal of Geophysical Research: Planets*, *122*, 771–783. https://doi.org/10.1002/2017JE005313

Radioti, A., Krupp, N., Woch, J., Lagg, A., Glassmeier, K.-H., & Waldrop, L. S. (2005). Ion abundance ratios in the Jovian magnetosphere. *Journal of Geophysical Research*, *110*, A07225. https://doi.org/10.1029/2004JA010775

Radioti, A., Woch, J., Kronberg, E. A., Krupp, N., Lagg, A., Glassmeier, K.-H., & Dougherty, M. K. (2007). Energetic ion composition during reconfiguration events in the Jovian magnetotail. *Journal of Geophysical Research*, *112*, A06221. https://doi.org/10.1029/2006JA012047

Saur, J., Duling, S., Roth, L., Jia, X., Strobel, D. F., Feldman, P. D., et al. (2014). The search for a subsurface ocean in Ganymede with Hubble Space Telescope observations of its auroral ovals. *Journal of Geophysical Research: Space Physics*, *120*, 1715–1737. https://doi.org/10.1002/2014JA020778

Saur, J., Strobel, D. F., & Neubauer, F. M. (1998). Interaction of the Jovian magnetosphere with Europa: Constraints on the neutral atmosphere. *Journal of Geophysical Research*, *103*(E9), 19,947–19,962.

Schreier, S., Eviatar, A., Vasyliunas, V. M., & Richardson, J. D. (1993). Modeling the Europa plasma torus. *Journal of Geophysical Research*, *98*, 21,231–21,243.

Shi, M., Baragiola, R. A., Grosjean, D. E., Johnson, R. E., Jurac, S., & Schou, J. (1995). Sputtering of water ice surfaces and the production of extended neutral atmospheres. *Journal of Geophysical Research*, *100*(E12), 26,387–26,395.

Smith, B. A., Soderblom, L. A., Beebe, R., Boyce, J., Briggs, G., Carr, M., et al. (1979). The Galilean satellites and Jupiter: Voyager 2 Imaging Science results. *Science*, *206*(4421), 927–950.

Speiser, T. W. (1965). Particle trajectories in a model current sheet, based on the open model of the magnetosphere, with applications to auroral physics. *Journal of Geophysical Research*, *70*(7), 1717–1728.

Spencer, J. R. (1987). Thermal segregation of water ice on the Galilean satellites. *Icarus*, *69*, 297–313.

Størmer, C. (1955). *The Polar Aurora*. New York: Oxford University Press.

Teolis, B. D., Loeffler, M. J., Raut, U., Famá, M., & Baragiola, R. A. (2006). Ozone synthesis on the icy satellites. *The Astrophysical Journal*, *644*, L141–L144.

Teolis, B. D., Plainaki, C., Cassidy, T. A., & Raut, U. (2017). Water ice radiolytic O_2, H_2, and H_2O_2 yields for any projectile species, energy, or temperature: A model for icy astrophysical bodies. *Journal of Geophysical Research: Planets*, *122*, 1996–2012. https://doi.org/10.1002/2017JE005285

Thomas, N., Bagenal, F., Hill, T. W., & Wilson, J. K. (2004). The Io neutral clouds and plasma torus. In N. Thomas, F. Bagenal, T. W. Hill, & J. K. Wilson (Eds.), *Jupiter: The planet, satellites, and magnetosphere* (pp. 561–591). Cambridge, UK: Cambridge University Press.

Tóth, G., Jia, X., Markidis, S., Peng, I. B., Chen, Y., Daldorff, L. K. S., et al. (2016). Extended magnetohydrodynamics with embedded particle-in-cell simulation of Ganymede's magnetosphere. *Journal of Geophysical Research: Space Physics*, *121*, 1273–1293. https://doi.org/10.1002/2015JA021997

Turc, L., Leclerq, L., Leblanc, F., Modolo, R., & Chaufray, J.-Y. (2014). Modelling Ganymede's neutral environment: A 3D test-particle simulation. *Icarus*, *229*, 157–169.

Vasyliunas, V. M., & Eviatar, A. (2000). Outflow of ions from Ganymede: A reinterpretation. *Geophysical Research Letters*, *27*(9), 1347–1349.

Volwerk, M., & Khurana, K. K. (2010). Ion pick-up near the icy Galileo satellites. In J. A. LeRoux, V. Florinski, & G. P. Zank (Eds.), *AIP Conference Proceedings* (Vol. 1302). Coates: American Institute of Physics.

Williams, D. J. (2001). Ganymede's ionic radiation belts. *Geophysical Research Letters*, *28*(19), 3793–3796.

Williams, D. J. (2004). Energetic electron beams in Ganymede's magnetosphere. *Journal of Geophysical Research*, *109*, A09211. https://doi.org/10.1029/2004JA010521

Williams, D. J., & Mauk, B. (1997). Pitch angle diffusion at Jupiter's moon Ganymede. *Journal of Geophysical Research*, *102*(A11), 24,283–24,287.

Williams, D. J., Mauk, B., & McEntire, R. W. (1998). Properties of Ganymede's magnetosphere as revealed by energetic particle observations. *Journal of Geophysical Research*, *103*(A8), 17,523–17,534.

Williams, D. J., Mauk, B. H., McEntire, R. W., Roelof, E. C., Armstrong, T. P., Wilken, B., et al. (1997). Energetic particle signatures at Ganymede: Implications for Ganymede's magnetic field. *Geophysical Research Letters*, *24*(17), 2163–2166.

Williams, D. J., McEntire, R. W., Jaskulek, S., & Wilken, B. (1992). The Galileo energetic particles detector. *Space Science Reviews*, *60*, 385–412.